



Molecular dynamics simulations of an electrified water/Pt(111) interface using point charge dissociative water



Kuan-Yu Yeh, Michael J. Janik*, Janna K. Maranas**

Department of Chemical Engineering, The Pennsylvania State University, Fenske Laboratory, University Park, PA 16801, United States

ARTICLE INFO

Article history:

Received 23 September 2012
Received in revised form 15 March 2013
Accepted 16 March 2013
Available online 25 March 2013

Keywords:

Aqueous solution–metal interface
Dissociative water
Proton transfer
Molecular dynamics
Water dipole relaxation

ABSTRACT

Water dissociation and structural diffusion of protons at the electrified water/Pt(111) interface are examined using molecular dynamics simulations. A combination of reactive water with a Pt(111) electrode under constant potential conditions is unique and relevant to fuel cell relevant electrochemistry. We use a modified central force model to describe reactive water and electrode charge dynamics to describe the electrode. We perform control simulations using SPC/E water, a contrast that clarifies when the influence of water ions on interfacial water structure and dynamics and electrochemical properties can no longer be neglected. Both mCF and SPC/E water have structured interfacial water layers regardless of electrode potential, but a reactive model is important when considering water structure away from the surface and interfacial dynamics. As opposed to SPC/E water, an applied potential does not induce preferred water orientation for mCF water in the middle of the electrolyte, despite the fact that interfacial OH and H₃O ions cannot completely screen the electrode potential. This occurs because fast exchanges among OH/H₂O/H₃O relax the electric field constraint in the surface normal direction. mCF water accurately describes the timescales of hydrogen bond vibration and structural diffusion of both hydronium and hydroxyl ions. This simple reactive water model distinguishes structural diffusion between H₃O and OH ions, where H₃O ion transfer is three times faster than OH ion transfer. The model allows us to determine the influence of applied potential and H₃O/OH ions on charge transfer effectiveness near the electrode surface, directly relevant to fuel cell electrochemistry.

© 2013 Elsevier Ltd. All rights reserved.

1. Introduction

The investigation of water structure and dynamics over metal electrodes is of interest in surface chemistry, electrocatalysis, and a wide range of energy applications, including fuel cells, batteries, and supercapacitors. The charged metal surface alters the arrangement, dielectric, and dynamic properties of water molecules near the surface, all of which play important roles in surface reactions and device efficiency. For instance, hydronium (hydroxyl) transfer to and from the electrode, which are crucial steps in acid (alkaline) fuel cells, requires appropriate water arrangement near the electrode [1–3]. However, the complex dynamic nature of the liquid/solid electrified interface makes it difficult to characterize experimentally. A realistic atomistic model to capture this interface also represents a substantial challenge for theoretical investigations.

Simulation of the aqueous electrolyte–electrode interface requires methodological choices that balance computational demands and accuracy for representing the electrochemical phenomena. Atomistic simulations provide insights into the preferential adsorption sites of water/ions, diffusion properties, and the electrostatic potential profile across the interface [1–6], all of which may impact electrode reaction rates and are not easily evaluated experimentally. With advances in computational power, ab initio molecular dynamics (MD) simulations are used to provide explicit treatment of electronic structure at the electrode/electrolyte interface [7–9]. However, ab initio MD schemes are currently too expensive to allow for simulations of sufficient length or size to capture electrochemical phenomena, such as ion distribution or the dynamics of water and ions under applied potentials. The use of molecular dynamics with parameterized force fields enables a dynamic description of the electrode/electrolyte interface on the appropriate time and length scales to provide statistically meaningful results.

To simulate an electrified metal electrode using classical MD simulations, different modeling approaches were developed. The key feature of the electrochemical interface is that an excess surface charge induced by an external potential attracts ions in the electrolyte to create a potential drop. The simplest approaches are

* Corresponding author. Tel.: +1 814 863 9366.

** Corresponding author. Tel.: +1 814 863 6228.

E-mail addresses: mjanik@engr.psu.edu, mjanik@psu.edu (M.J. Janik), jmaranas@psu.edu (J.K. Maranas).

to apply a constant electric field across the entire electrolyte [1,6] or evenly distribute a constant charge density on a wall-like plane [10–12]. Metal surfaces are not structureless planes, and water molecules have preferential adsorption sites, resulting in an inhomogeneous surface charge distribution induced by the ions or polar solvents [4]. In addition, these approaches limit the representation of electrolyte/metallic electrode interactions because metal polarizability is not taken into account and metal electrodes are more often operated as constant-potential rather than constant-charge surfaces. Modeling metal electrodes with a potential controlled approach and an atomistic-level description of surface topology would allow simulations of metal electrodes that better parallel controlled potential experiments.

To account for metal polarizability, image charge methods have been developed [13,14]; however, image-charge methods can only simulate a charged electrode that corresponds to the net charge in the electrolyte, which makes it difficult to represent constant potential conditions at various ion concentrations. Fluctuating charge methods, which address the metal polarizability as the image charge method and maintain charge neutrality in both electrolyte and electrode, enables a potential controlled electrochemical interface. A polarizable charged plane that maintains a constant potential has been developed by Siepmann and Sprik [15] using a Gaussian charge distribution to represent conduction band electrons on each metal atom. These electrons can be transferred between atoms within the electrode. To respond to charges in the electrolyte, the charge on each metal atom is reassigned through the minimization of total electrostatic energy at each time step. This method has been modified and extended to MD simulations, representing the features of water and salt solution near an electrode surface [4,16]. The electrode charge dynamics (ECD) method, developed by Wheeler and co-workers [5], uses a similar description of charge fluctuation under a constant potential condition and a simple representation of water–metal interactions. We use the ECD approach in this study.

Under the influence of strong electric fields (typical magnitude 10^8 V m^{-1}), at the electrochemical interface, water in the electrolyte will dissociate [17,18], and could oxidize at the electrode surface [19]. The influence of H_3O^+ and OH^- , referred to as water ions [20], on structural and dynamic properties of the electrochemical interface and the structural diffusion of water ions near the electrode has been neglected in most classical force field simulations because a dissociative water model is required. In addition, the influence of applied potential on the dynamics and dielectric properties of dissociative water in the vicinity of the electrode has not been addressed. There is a need to construct a more realistic electrochemical interface, where dissociative water molecules are interacting with potential controlled electrodes.

Dissociative (reactive) water force fields are mainly aimed at studying proton transfer in solution [21–26], where bond breaking and formation is required to model structural diffusion (Grothuss mechanism) [27]. A variety of reactive water models involving different levels of complexity have been applied to proton transfer in bulk water [21,22,24,28] and polymer membranes [29,30]. In some models, a procedure is used that initiates proton hopping based on the satisfaction of geometric and energetic criteria [24], or establishes proton transfer based on probabilities tied to energy barriers [25]. These models have made significant contributions toward the understanding of solvated structure and proton dynamics and revealed that the proton transfer mechanism in bulk solution is different than that in confined environments, such as polymer electrolytes [30] or carbon nanotubes [23]. A few MD studies have focused on proton transfer at the electrochemical interface. Spohr and co-workers studied proton transfer near a platinum electrode using a multistate empirical valence bond (MS-EVB) approach [31].

In this approach, bond formation and breaking are described by energy states that enable the model to capture electron transfer. This sophisticated model was used to characterize proton discharge kinetics under constant surface charge conditions. The influence of oxygen species from water dissociation (OH^- , adsorbed O and OH), which could alter the proton transfer mechanism near the surface [19], is neglected. A simple reactive water model that allows us to model OH and H_3O ions without additional force field parameterizations and balance the computationally demanding description of the metal electrode would be useful to investigate the influence of water ions on proton transfer dynamics under constant potential conditions.

The simplest reactive water model, the central force (CF) model, developed by Lemberg, Stillinger and Rahman [32,33] uses simple point charges with pairwise interactions. Recently, Hofmann et al. [34] parameterized a set of pairwise water potentials using experimental pair distribution functions of liquid water. The resulting potentials are similar to the original CF model. CF-type models can describe the structure, self-diffusion coefficient, and static dielectric constant of liquid water [35,36]. Hofmann's CF model also succeeded in predicting proton transfer dynamics in Nafion [37]. We therefore apply a CF-type model to provide structure and dynamics of water and water ions over the electrode surface, with adaptations as discussed in the next section. Using this simple model, we are able to provide a realistic representation of interfacial electrochemical phenomena with less computational demand compared than quantum calculations or high-level MD approaches where electrolyte polarizability is taken into account.

In the present work, we report water/metal interface molecular dynamics simulations that include two key features: (1) water dissociation, which is taken into account using a simple CF-type water model, and (2) a polarization of the electrode that allows a preset potential drop across the electrolyte. We describe a modification to the original-CF model [32,33] in order to improve water reactivity and implement the modified CF and SPC/E models with the ECD method [5]. To address the importance of water dissociation, we carry out control simulations with the extended simple point charge (SPC/E) water model [38]. The comparison between dissociative water and SPC/E water suggests that water ions affect electrochemical properties, such as capacitance and dielectric constant, although interfacial water structure and dynamics are similar in both models. We also show that structural diffusion in hydronium and hydroxyl transfer is affected by the interfacial ion distribution. Our findings indicate the importance of accounting for water dissociation when modeling an aqueous electrochemical interface.

2. Model development and simulation details

2.1. Force field development

The water model in this study provides a simple but realistic interaction that includes bond breaking/formation of liquid water between Pt electrodes. The original-CF model reliably describes liquid water, but predicts a small diffusion coefficient [33], as shown in Table 1. As was observed in Ref. [33], we find that all water molecules (200 H_2O at 300 K) remain intact when using the original-CF model in the absence of an applied potential. If the simulation is initiated with one dissociated water molecule and 199 intact water molecules, recombination of H and OH does not occur during 2 ns, and H atoms are attached to the same oxygen atom in OH, H_2O , and H_3O throughout this time. Thus, inter-conversion between covalent and hydrogen bonds never occurs.

Table 1
Comparison between water force field models.

	Rigid water model	Central force model	Experiments
	SPC/E	Modified Original	
Molecular properties			
Charge on H atom (e)	0.42380	0.329830	
Equilibrium OH distance (nm)	0.1	0.096	0.096
Average HOH angle (°)	109.45	98.35	99.97
Average water dipole moment ^a (D)	2.35	2.24	2.27
Bulk properties			
Diffusion coefficient ($\times 10^{-5}$ cm s $^{-2}$)	2.52	2.44	1.05
			2.3 [42]

^a The average dipole moment is calculated using the equilibrium OH distance and average HOH angle.

The energy barrier associated with proton transfer can be estimated from the potential of mean force, $W(r)$, between oxygen and hydrogen atoms:

$$W_{\text{OH}}(r) = -k_B T \ln(g_{\text{OH}}(r)) \quad (1)$$

where $g_{\text{OH}}(r)$ is the pair distribution function of an OH pair, and k_B represents the Boltzmann constant. In Fig. 1(a) we present the potential of mean force obtained from the original-CF model, where a barrier larger than 62.7 kJ mol $^{-1}$ is observed in OH distances separating covalent and hydrogen bonded OH pairs (0.10–0.16 nm). A modification that reduces this energy barrier is needed to allow transfer events to occur. As a target, we use the potential of mean force estimated from the experimental $g_{\text{OH}}(r)$ [39], which has a barrier of 10.5 kJ mol $^{-1}$. Adjusting the O–H interaction to match this barrier also influences OO and HH interactions, and thus these potentials also need modification. The resulting set of CF potentials is given in Eqs. (2)–(4). This modified CF model, denoted as the mCF model, gives reasonable agreement with the barrier for proton transfer as well as all three pair distribution functions, as shown in Fig. 1.

To examine the effect of water dissociation on the properties of the water/metal interface, the SPC/E water model is also used. Compared with $g(r)$ s from neutron diffraction experiments [39], the SPC/E model more closely agrees with the first peak positions for $g_{\text{OO}}(r)$ and $g_{\text{HH}}(r)$ than the mCF model, although the reverse is true for $g_{\text{OH}}(r)$. Structural differences in going from the CF to the mCF model lead to a reduced water angle and thus water dipole moment whereas the mCF water self-diffusion coefficient is improved over the original-CF model. Bulk water properties of SPC/E, mCF, and original-CF water models are summarized in Table 1.

$$\phi_{\text{HH}}(r) = \frac{15.1042}{r} + \frac{75.24}{1 + \exp[275(r - 0.1975)]} - 69.64 \exp[-762.177(r - 0.145252)^2] \quad (2)$$

$$\phi_{\text{OH}}(r) = \frac{-30.2084}{r} - \frac{8.36}{1 + \exp[54.9305(r - 0.22)]} - \frac{8.36}{1 + \exp[400(r - 0.105)]} + \frac{1.647 \times 10^{-8}}{r^{9.19912}} \quad (3)$$

$$\phi_{\text{OO}}(r) = \frac{60.4168}{r} - 1.045 \exp[-150(r - 0.45)^2] - 1.045 \exp[-400(r - 0.34)^2] + \frac{5.5792 \times 10^{-5}}{r^{9.302055}} \quad (4)$$

The force-field modeling approach we use for potential-controlled electrodes is based on the ECD model [5]. Pt(1 1 1) is chosen as the electrode because Pt is the most commonly used catalyst for proton-exchange membrane fuel cells and (1 1 1) is its most

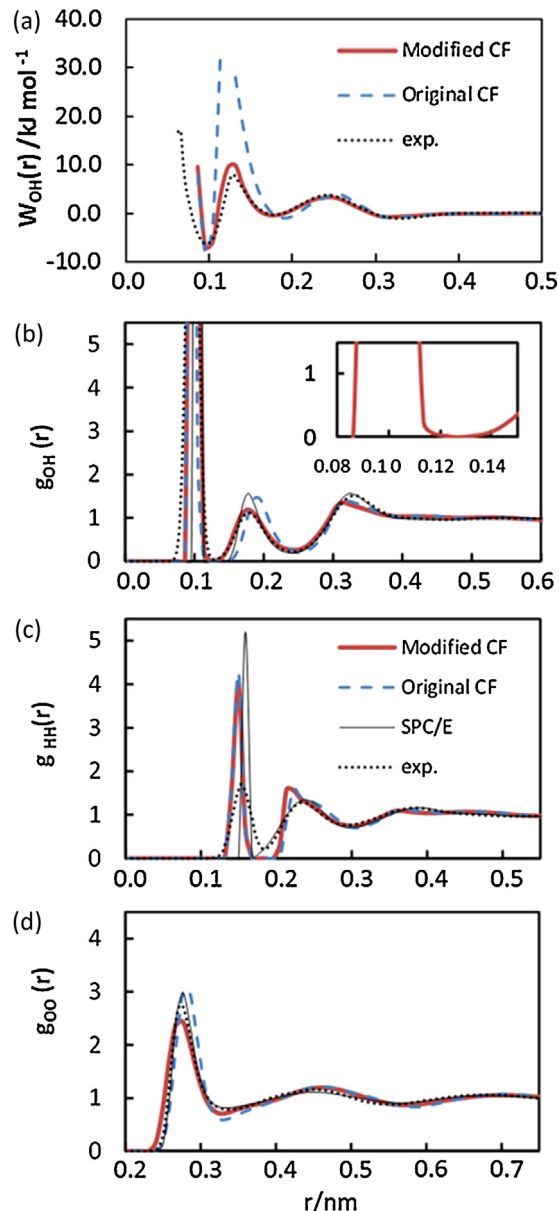


Fig. 1. (a) Potential of mean force of oxygen–hydrogen pair, and pair distribution functions of (b) oxygen–hydrogen, (c) hydrogen–hydrogen, and (d) oxygen–oxygen for a bulk water simulation at 300 K. Results are shown in the solid lines (red) for the modified-central force model, dashed lines (blue) for the original-central force model, and thin (black) lines for the SPC/E model. Experimental data from neutron diffraction [39] are shown in the dotted lines (black). The inset in (b) shows the enlarged first peak of $g_{\text{OH}}(r)$ to determine the cutoff distance that defines a chemical bond between O and H.

stable surface facet. The ECD model adopts a fluctuating charge scheme, where each Pt atom carries a fixed nuclei charge (point charge) and a Gaussian-shaped valence electron distribution. An offset potential sets different voltages over the Gaussian-shaped valence charge, creating a potential difference between two electrodes, which are presented as two halves in a large 2-d slab. The magnitude of the Gaussian charge changes in response to the atoms in the electrolyte and the applied offset while maintaining a constant potential condition in each slab half. This is accomplished by adjusting the magnitude of Gaussian charge distributions by minimizing the total electrostatic energy at each time step. Solving a linear minimization problem at each time step is computational time consuming. Wheeler's group developed an alternative implementation where the valence electrons are treated as dynamic degrees of freedom with fictitious masses and velocities that can be integrated into a time evolution scheme, as described in Ref. [5]. The ECD scheme has been implemented into a modified version of LAMMPS (Large-scale Atomic/Molecular Massively Parallel Simulator) simulation package by Payne et al. [43,44]. ECD methods require two parameters for each ECD atom: the magnitude of the core charge and the inverse Gaussian width for valence electrons. We use the parameters provided in Ref [44]: a core charge of 1.0 |e| and 0.0751 nm⁻¹ for the inverse width. In the ECD method, platinum–platinum interactions (nuclei–nuclei, nuclei–electron, and electron–electron) are purely electrostatic, as described in detail in the original paper [5].

To describe interactions between water and Pt, the ECD method uses both Coulombic interactions and a short-range interaction in the form of a modified-Morse potential. The ECD method does not allow charge transfer between the metal slabs and the O/H atoms.

The water-Pt short range interaction was parameterized using density functional theory (DFT) calculations, in which we varied the Pt–O distance for four different water orientations at a top site of the Pt(1 1 1) electrode. We only use top sites because the most favorable water orientation on a Pt(1 1 1) surface is parallel to the surface above the top site [45,46]. The DFT calculations were performed with a 3-layer 3 × 3 Pt(1 1 1) unit cell using the Vienna Ab initio simulation package (VASP) [47–49]. The PAW-GGA approach [50] and the PW91 exchange-correlation functional [51,52] were used. Water–Pt interaction energies in the ECD approach were calculated by placing water molecules over the Pt(1 1 1) electrode. To extract the parameters for modified Morse potentials (Eqs. (5) and (6)), the sum of Coulombic and H/O modified-Morse interactions from ECD calculations are fit to the DFT results. Regardless of the Pt–O distance, the energy is dominated by the modified-Morse interaction. The charge and OH/HH pair interaction difference between the SPC/E and mCF water model has little influence on the ECD interaction energies, hence the two water models share the same set of water–platinum potentials. Fig. 2 shows ECD energies are generally in good agreement with DFT results. However, the hydrogen-down adsorption configuration ($\theta_\mu = 180^\circ$) at large Pt–O distance is not favorable for the ECD model. The difficulty in accurately capturing water adsorption in all orientations is due to the small number of adjustable parameters available in modified Morse potentials.

$$\phi_{\text{Pt}-\text{O}}(r) = -3.5426[1 - [1 - \exp(-13.50(r - 0.2890))]^2] \quad (5)$$

$$\phi_{\text{Pt}-\text{H}}(r) = -0.8423[1 - [1 - \exp(-13.03(r - 0.3351))]^2] \quad (6)$$

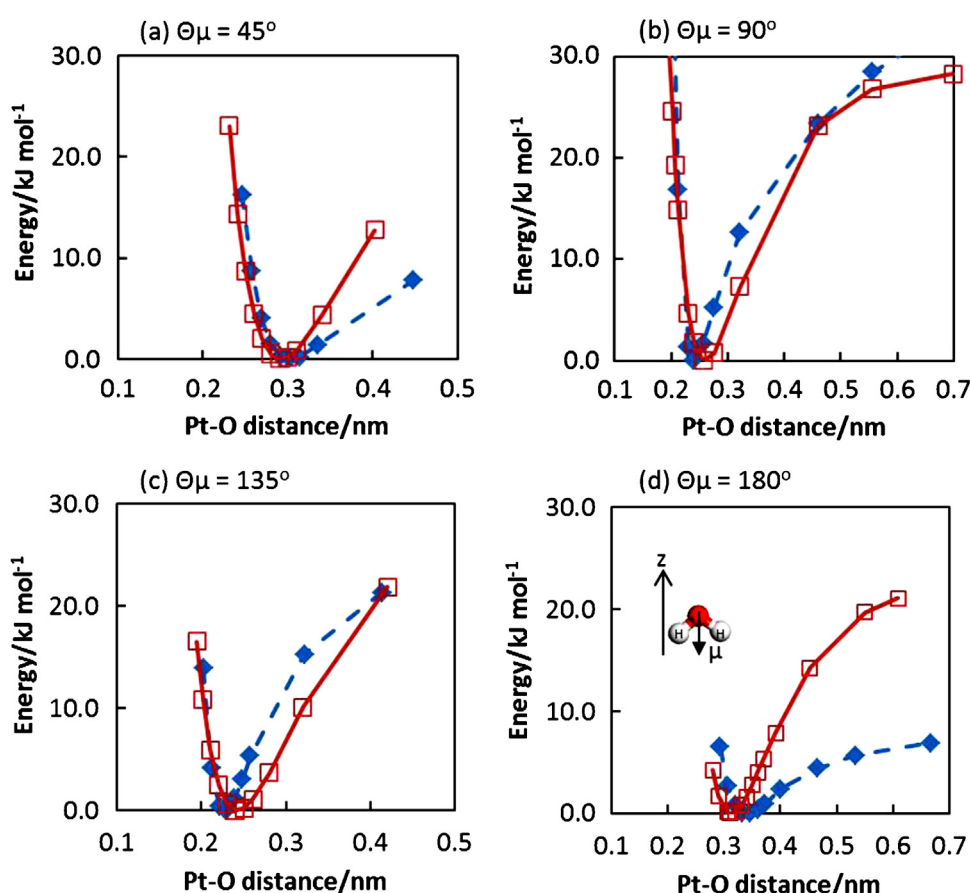


Fig. 2. Comparison of ECD (□ with solid lines) and DFT (◆ with dashed lines) calculated energies of different water orientations at a top site of the Pt(1 1 1) electrode: (a) $\theta_\mu = 45^\circ$, (b) $\theta_\mu = 90^\circ$, (c) $\theta_\mu = 135^\circ$ and (d) $\theta_\mu = 180^\circ$ (H-down). θ_μ is the angle between water dipole vectors (from O to H) and the surface normal direction.

2.2. Simulation details

All simulations are performed using the LAMMPS simulation package [53,54]. Bulk water simulations are composed of 200 water molecules in a $1.8177\text{ nm} \times 1.8177\text{ nm} \times 1.8177\text{ nm}$ cubic cell using a NVT simulation. Long-range Coulombic interactions are calculated using the Ewald sum method. The equations of motion are solved using the Verlet algorithm [55] with a time step of 2 fs for SPC/E and 0.25 fs for mCF models. Temperature (300 K) is maintained via a Nose-Hoover thermostat [56,57] with a time constant of 100 time steps. We use equilibrated SPC/E water as an initial structure for mCF water simulations. Restructuring of mCF water occurs very rapidly and a new stable state is quickly reached. Thus, we equilibrate mCF water for the same time (1 ns) required for SPC/E water [58]. Production runs of 4 ns follow the equilibration period.

The water/Pt interface simulations are carried out for 650 water molecules between Pt(1 1 1) electrodes, as shown in Fig. 3. The electrode consists of a rigid slab of 392 platinum atoms arranged in a seven layer Pt(1 1 1) slab, where the Pt atoms on the 1st and 7th layers (surface layers) are in the same arrangement. The thickness of seven layers is larger than short range cut-off distance used in our simulation and able to avoid water near the 1st Pt layer interacting with water near the 7th layer. The simulation cell is a tetragonal box of $1.9403\text{ nm} \times 1.9204\text{ nm} \times 6.52745\text{ nm}$ with periodic boundary conditions in all directions. The choice of system size is based on the simulation cut-off distance of 0.9 nm for short range interactions and water Bjerrum length of 0.7 nm. Also, a sufficient length for z-direction to represent the bulk region is chosen based on a previous simulation of water over a Pt electrode [2].

The 7-layer metal slab serves as two opposite electrodes where the 1st to 3rd layers form the negatively charged electrode and the 4th to 7th layers form the positively charged electrode. A constant potential offset is applied by adding a constant offset between the

energy of valence electrons on the “left” (layers 1–3) and “right” (layers 4–7) electrodes. For example, the energy of valence electrons in the right electrode is set 1.25 eV higher than the left half, giving an average potential difference of 1.25 V between the halves of the Pt slab and creating a potential drop across the water layer, as shown in Fig. 3. We apply potentials of 0, 1.25, 1.875 and 2.5 V in this study. An applied potential leads to charge redistribution in the metal layers, similar physically to placing a potentiostat between two electrodes to maintain a constant potential difference during an experiment. However, what is not physically accurate to a typical electrochemical system is that the two electrodes are placed “back to back” in our model due to the periodic boundary conditions. To assure that this proximity does not alter the measured phenomena at the interface or in the electrolyte region, we tested slabs with 10 layers for a subset of simulations and found no noticeable difference.

The potential difference is applied by changing the relative energy of valence electrons between the two adjacent halves of the metal slab. The discrete delta function of the core charge causes potential oscillations in the total charge distribution and thus in the electric potential profile. The potential drop is clearly seen between the two connected electrodes, as shown in Fig. 3. The potential oscillations through the metal layers of each electrode occur on passing from the positive layers of concentrated nuclei point charges to the interstitial negatively charged layers. This does not reflect the classical picture of a flat potential within a conductor due to the distinct representation of Gaussian negative charges and local positive atom centers. The electrode potential difference, which is defined by the average potential difference between the electrodes, is controlled by the preset voltage difference on the valence electrons.

To avoid coulomb interactions between periodic images in the surface normal direction, the 2D, rather than 3D, Ewald sum should be used for long range interactions. ECD methods use variable

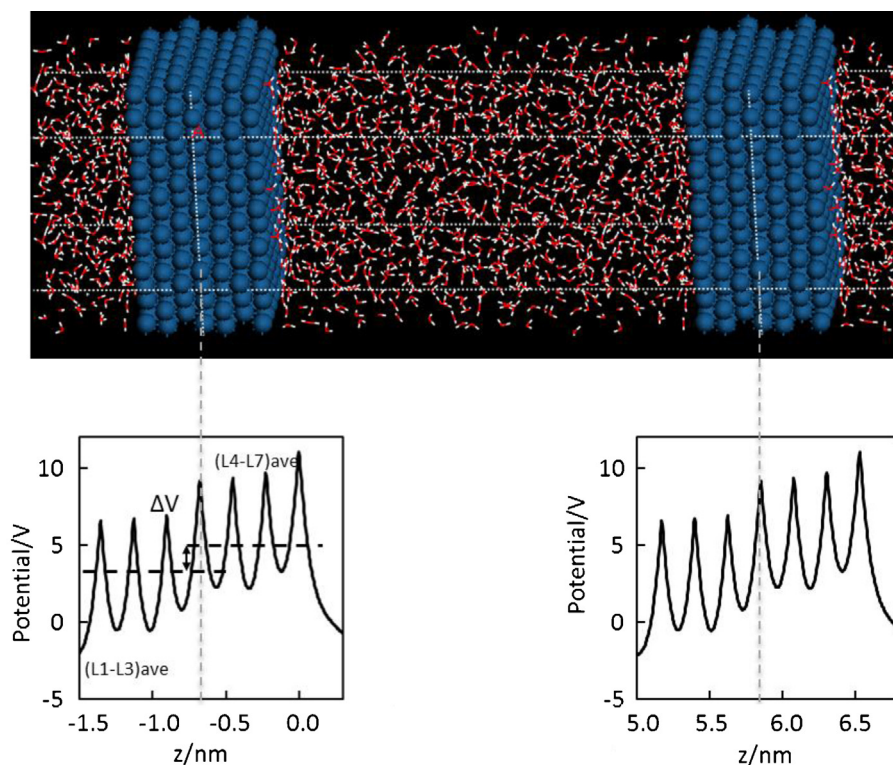


Fig. 3. The simulation cell: the simulation cell consists of 650 water molecules between two platinum electrodes held at a constant electrode potential offset ($\Delta V = 1.25\text{ V}$) (blue: Pt atoms, red (dark): O atoms, and white: H atoms). The dashed lines represent the periodic boundaries. The bottom panels show the electric potential profiles within the Pt slab. As detailed in the text, the applied potential drop in the ECD model is the average potential difference between the two electrodes. (For interpretation of the references to color in this figure legend, the reader is referred to the web version of this article.)

valence electrons to account for metal polarizability. The mobile electrons constitute conductor behavior of the metal electrode and are thus able to properly shield an external electric field from ions in other periodic images in the surface normal direction. Therefore, we can directly apply 3D Ewald sum to our system, as discussed in Ref. [5].

MD simulations at the water/Pt interface were carried out using Canonical ensemble (NVT). The temperature was set at 300 K and the volume was chosen to give a density of 1 g cm⁻³ in the bulk region of the water layer. The particle-particle-particle-mesh (PPPM) technique is used to compute long-range Coulombic interactions [59]. The time step of SPC/E water over the Pt electrode is 1 fs. The simulations for SPC/E water system are allowed to equilibrate for 2 ns followed by data collection for 8 ns. For mCF water over the Pt electrode, we use a time step of 0.25 fs. The simulations for mCF water are allowed to equilibrate for 2 ns followed by production runs are 5 ns. Temperature is controlled by the Nose-Hoover thermostat [56,57] using a time constant of 100 timesteps for both SPC/E and mCF water. For the valence charge degree of freedom, a separate Nose-Hoover thermostat is applied with a time constant of 100 timesteps and temperature of 5 K [5].

3. Results and discussion

3.1. Water ion density profiles

The improved water reactivity of the mCF model is evidenced by the observation of water dissociation events during a bulk water MD simulation. In order to facilitate chemical interpretation of species encountered during the MD simulations, it is useful to introduce a cutoff distance that defines a chemical bond between O and H. We choose this distance (0.13 nm, see inset of Fig. 1(b)) such that the bond included the entire first peak of the O–H pair distribution function. The number of H atoms within the cutoff distance of a given oxygen atom determines its identity. Using this definition, the solution consists of 94% H₂O, 3% OH, and 3% H₃O, in agreement with the results of a recently developed CF-type water model (90% intact water) by Hofmann et al. [34]. Because of the simplified use of fixed charges and the lack of many-body interaction terms, the CF-type of model has inevitable inaccuracies. To address the capability of capturing proton transfer within an electrolyte solution, the degree of water self-ionization is compromised. However, the definition of ion species (use of an O–H cutoff distance with an instantaneous measurement) and thus ion concentration in the simulation differs from the experimental measurement, making direct comparison with experimental water self-ionization values difficult. We have found that our model is useful to examine proton distribution and dynamics in an acidic/basic electrolyte solution adjacent to an electrode surface.

The density profiles of atoms and ions are important structural properties of the electrochemical interface. When mCF water is in contact with Pt electrodes, the interplay between water ions and the electrode creates a different interfacial structure than SPC/E water. Fig. 4 shows the density profiles of H₃O and OH ions in mCF water. The ion density is reported as the ratio of the local density relative to the bulk density of that species determined from solution simulations. Within the simulated unit cell, the left hand side of the electrode ($z < 0.0$ nm) is positively charged (positive potential), and the right hand side of the electrode ($z > 5.17$ nm) is negatively charged (negative potential). As mentioned above, 6% of mCF water dissociates into OH and H₃O in the absence of a Pt electrode. The solution composition remains the same when mCF water is in contact with the electrode at $\Delta V = 0$. However, even without any applied potential, more H₃O (Fig. 4(a)) ions accumulate at the right hand side (negative) of the electrode surface and

more OH (Fig. 4(b)) ions accumulate on the left hand side (positive) such that a slight asymmetry exists in the system.

Applied potentials induce greater water dissociation, create additional ion peaks, and increase the amplitude of the hydronium and hydroxyl density oscillations. Although our model does not allow electron transfer between electrode and electrolyte, the strong electrostatic interaction with an increased potential is able to motivate water dissociation over the electrode surface. Fig. 4 shows two snapshots from the simulation systems: in (c) one hydronium is adsorbed at the negatively charged surface, and in (d) two hydroxyls ions are adsorbed at the positively charged surface. The number of dissociated water molecules increases from 33 to 47 when $\Delta V = 0$ increases from 0 to 2.5 V. We also observe three to five oxygen atoms embedded within positively charged Pt layers when potentials of 1.875 and 2.5 V are applied. The small amount of oxygen charge has little influence on the overall electrode potential. In the bulk electrolyte region ($z = 1.5$ –3.5 nm in Fig. 4(a) and (b)), the density of OH and H₃O remains constant as electrode potential varies, but the bulk concentrations of OH ion are slightly higher than those of H₃O, indicating that complete electrostatic screening has not been achieved. Near the electrode surface, different interfacial structures of hydronium and hydroxyl are observed. For hydroxyl ions near positively charged surfaces (left-hand-side in Fig. 4(b)), OH ions remain very strongly adsorbed to the surface. With an increased potential, the OH density peak is shifted toward closer to the surface, creating broad peaks and further stabilizing the interfacial structure. On the contrary, hydronium peaks near negatively charged surfaces (right panel in Fig. 4(a)) are sharper and narrower than hydroxyl peaks on positively charged surfaces, and more hydronium peaks are formed. The position and width of the first hydronium peak is insensitive to the applied potentials, as observed in ab initio MD studies [8]. The distinct behavior observed between the two electrodes reflects the different interaction between cation-water and anion-water. The asymmetric water density and orientation due to applied potentials also results in asymmetric OH and H₃O distribution, as discussed in the following sections.

3.2. Comparisons of interfacial water structure and orientation between SPC/E and mCF water models

The arrangement of water molecules near a charged surface distinctly differs from that of bulk water. Molecular dynamics simulations [10–12,60] predict that water molecules arrange in two to three layers adjacent to a crystalline metallic surface with density different from the bulk because of the disruption of the hydrogen bond network in the surface layer [61]. A potential dependent reorientation of surface water due to the interaction of water dipoles with an applied field has also been reported [1,4,6,11,60]. The impact of hydronium and hydroxyl ions on water structure at the water/metal interface leads to different density and thus electrical potential profiles. To investigate the role of water ions, we compare identical systems, simulated with non-dissociative SPC/E and dissociative mCF water models. The mCF water model also has additional degrees of freedom associated with bond and angle flexibility of water molecules. The different interfacial structure between these two water models also illustrates the influence of water polarizability in terms of bond flexibility.

Interfacial water packing is evaluated using oxygen density profiles. Orientational ordering of the water dipole is evaluated using a orientational order parameter (P) [62], defined by

$$P(z) = \left\langle \frac{1}{N(z)} \sum_{i=1}^N \frac{(3\hat{\mu}_{z,i}^2 - 1)}{2} \right\rangle \quad (7)$$

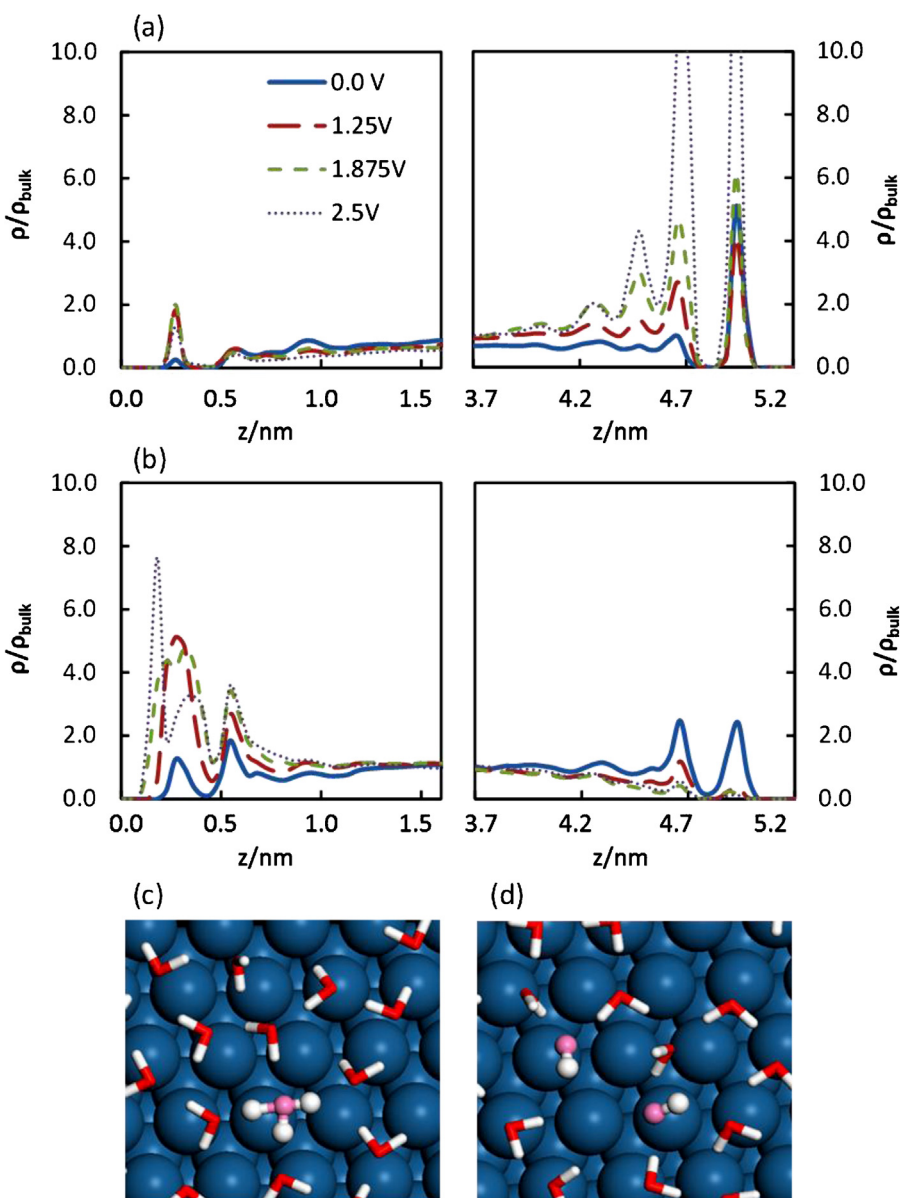


Fig. 4. Interfacial density profiles of (a) hydronium and (b) hydroxyl ions at various applied potentials. (c) and (d) are snapshots from negatively (c) and positively (d) charged surfaces under a potential offset of 1.25 V. Atoms shown in ball and stick format highlight the ion species.

where $\widehat{\mu_{z,i}}$ is the unit vector associated with a water dipole moment μ in the surface normal direction, N is the total number of water molecules in the system, and $\langle \rangle$ signifies a time average. The order parameter represents the average water dipole orientation, which can be analyzed for any specific region within the solution layer. Under this definition, the parameter P approaches zero when water molecules are randomly orientated in all three directions. $P = -1/2$ or 1 indicates that water dipoles are exclusively parallel to the surface ($\theta_\mu = 90^\circ$) or parallel to the $+z$ direction ($\theta_\mu = 0^\circ$). We applied the same definition on both surfaces: for $P = 1$, water molecules are in a H-up orientation on the positively charged surface or in a H-down orientation on the negatively charged surface. For mCF water, we only consider oxygen coordinated with two hydrogens within the predefined cutoff distance and a HOH angle less than 120° as an intact water molecule to ensure we capture the behavior of water molecules rather than dissociation intermediates.

Water layering and orientational ordering strongly depend on the location of water molecules along the surface normal direction. Figs. 5 and 6 compare the oxygen density profiles and ordering

parameters obtained from mCF and SPC/E water simulations for various applied potentials. We first discuss the results of zero applied potential. Under $\Delta V = 0$ V, oxygen density distributions from both mCF and SPC/E water models agree with previous studies of water over a Pt(1 1 1) electrode [10–12,60], where a well-defined first layer, a diffuse second layer and traces of a third water layer comprise an interfacial region of approximately 1.0 nm, as shown in Fig. 5(a). Comparing the left and right panels in Fig. 5(a), the slight asymmetry of the oxygen profile of mCF water is due to accumulation of water ions near the right hand side of the surface. Water orientation, in terms of order parameters as shown in Fig. 6, is closely related to water layering. At the first oxygen peak near both electrodes, $P(z)$ is negative, indicating that the majority of water dipoles are parallel to the surface. This orientation restriction occurs because water molecules preferentially orient parallel to the surface to maintain maximum interaction and formation of H-bonds with the surface [63]. The order parameter is much smaller in the second water layer, indicating a more random water orientation compared to the first layer. A bulk-like behavior

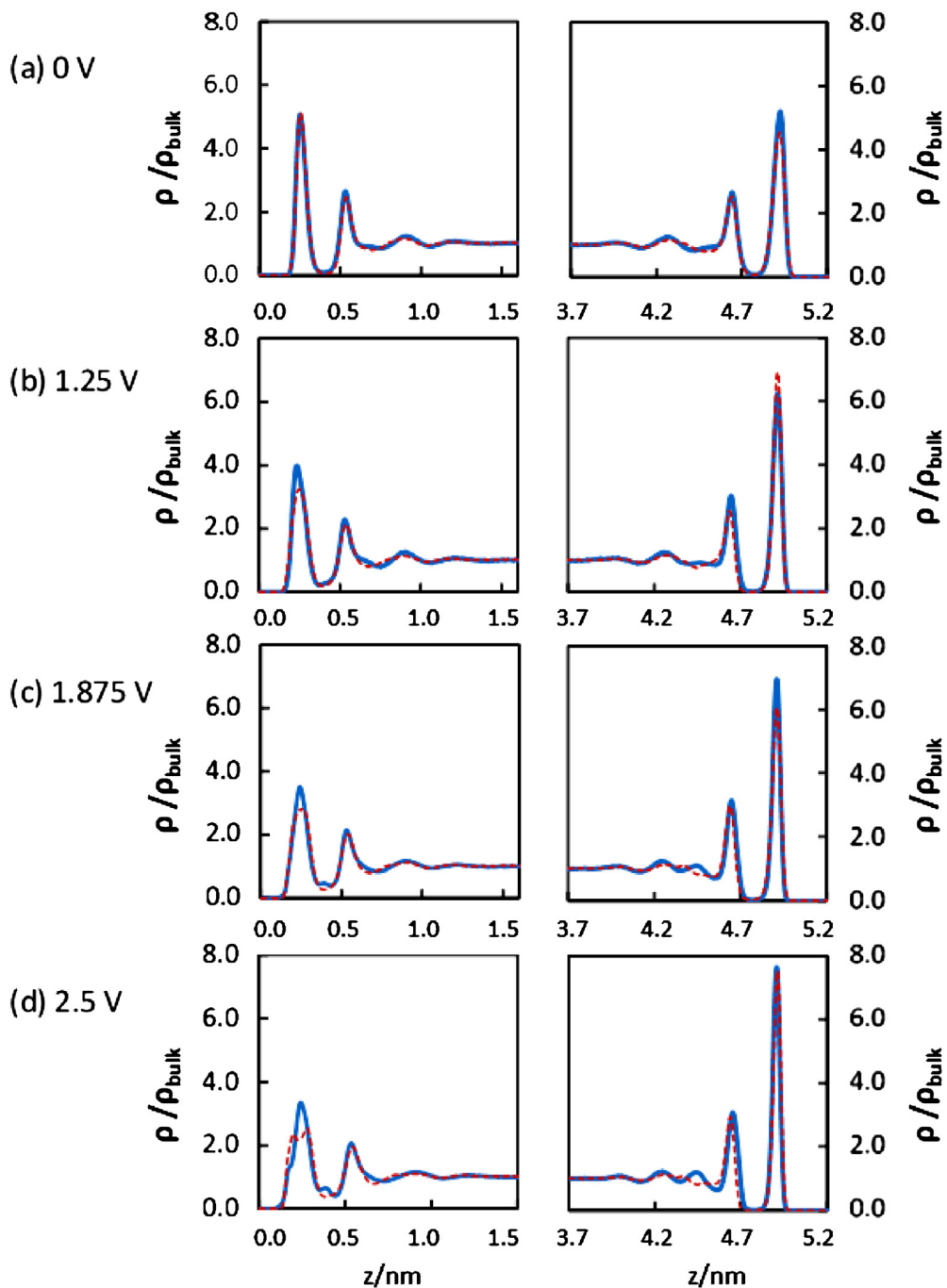


Fig. 5. Comparison of oxygen density profiles from mCF water (solid – blue lines) and SPC/E water (dashed – red lines) under applied potentials of (a) 0 V, (b) 1.25 V, (c) 1.875 V, and (d) 2.5 V. Left panels are results near positively charged surfaces ($z=0.0 \text{ nm}$), and right panels are results near negatively charged surfaces ($z=5.2 \text{ nm}$).

with random dipole orientations ($P=0$) appears at 1.0 nm away from the surface, consistent with the oxygen density profile. The similar density and orientation profiles from both water models indicate that bond flexibility in the mCF water model has little effect on interfacial structure, which is mostly driven by short range water–platinum interactions that do not differ between models.

Applied potentials have similar influence on oxygen density profiles of mCF and SPC/E water, whereas the influence on water orientation is significantly different. As observed in previous studies [1,6,31,64], the influence of applied potentials on the surface water layer is most prominent, and thus we focus on that layer. We first discuss the results near positively charged surfaces. As

seen in the left panel in Fig. 5, increasingly positive surfaces attract the negatively charged oxygen, orienting surface water molecules (Fig. 6) and broadening the first density peak (Fig. 5). The increased peak height for mCF water indicates the formation of more structured surface layers. This results from accumulation of hydroxyl anions and the increased bond flexibility [11,65] of mCF water. At $\Delta V=2.5 \text{ V}$, the first peak for SPC/E water splits into two sublayers. This has distinct orientational characteristics; water molecules in the first sublayer orient in H-up configurations, whereas those in the second sublayer orient parallel to the surface. Peak splitting occurs in SPC/E water because the H-up water configuration in the first sublayer minimizes the electric field/dipole interaction and stabilizes the electrostatic interaction between water and

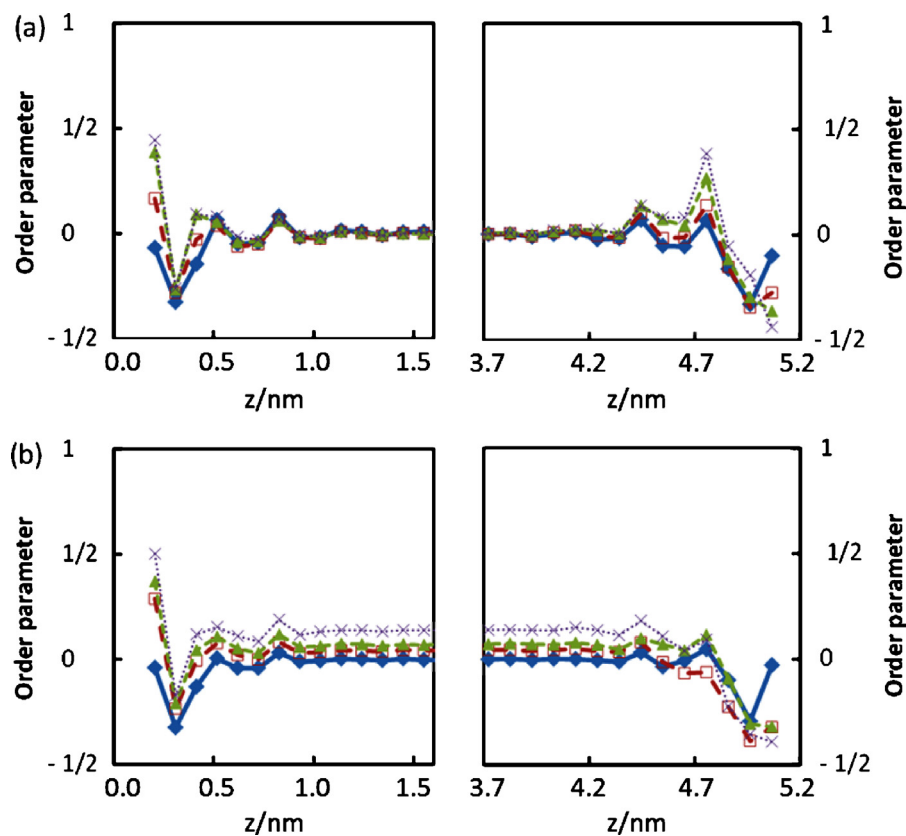


Fig. 6. Comparison of water dipole orientational parameters, P , from (a) mCF water and (b) SPC/E water under applied potentials of 0 V (♦), 1.25 V (□), 1.875 V (▲), and 2.5 V (×). $z=0$ represents positively charged surfaces, and $z=5.2$ nm represents negatively charged surfaces.

the electrode. The peak splitting is not prominent in mCF water because ionic species can effectively screen the local field.

Negatively charged surfaces have the opposite influence on water orientation (right panels in Figs. 5 and 6). As noted in Section 2, our Pt–H potential hinders the H-down configuration ($\theta_{\mu} = 180^\circ$). Even at the most negatively charged surface ($\Delta V = 2.5$ V), the strong electrostatic interaction is not sufficient to overcome the energy barrier for water reorientation into the H-down configuration, as seen in the nearly $-1/2$ order parameter in Fig. 6 right panel. Instead, water molecules form a packed surface layer to stabilize the negatively charged electrode. Hydroniums do not permit as much reorientation of the water due to strong solvation. The similarity of oxygen distribution between SPC/E and mCF water under applied potentials indicates the presence of OH and H_3O has little effect on interfacial water structure.

The most distinct difference in orientational ordering between SPC/E water and mCF water appears in the bulk region where the order parameter of mCF water vanishes when a potential is applied. For SPC/E water, an applied potential leads to orientational ordering of water dipoles (non-zero P) in the bulk solution region [4,6]. Thus, SPC/E water in the center of the simulation cell experiences a field inducing preferential orientation of the rigid water molecules and an appreciable dipole potential opposite the direction of the applied potential. Under a 2.5 V applied potential, the order parameter in the bulk region of SPC/E water ($P=0.14$) corresponds to an average angle of 65° between the water dipole and the surface normal direction. In the same situation, the order parameter of mCF water is negligible, indicating applied potentials have no effect on the bulk water orientation. This might be due to ion formation and molecular flexibility (polarizability) of mCF water that enhance water dipole ordering near the electrode surface, leading to larger screening [11,65] than rigid SPC/E water. The resulting electrostatic

potential distributions, from collective effects of an applied potential, water polarizability and ion formation, are examined in the following section.

3.3. Electrostatic potential

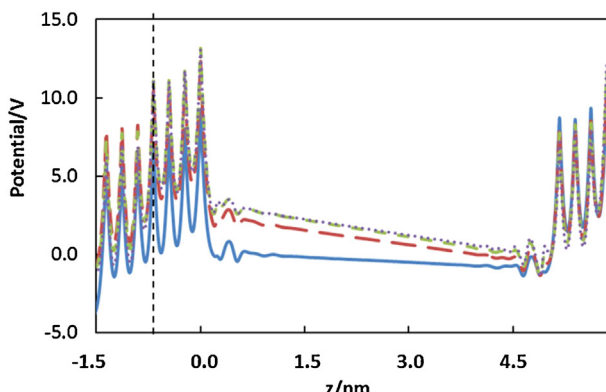
The x – y plane mean electric potential (V) across the simulation cell can be calculated from the mean charge density (ρ) via Poisson's equation

$$\nabla^2 V_z = -\frac{\rho(z)}{\varepsilon_0} \quad (8)$$

where ε_0 is the vacuum permittivity. The mean charge densities are obtained from the atom density profiles by multiplying by the charge on each atom. As mentioned in Section 2, the constant electrode potential is defined by averaging the potential oscillation within each electrode. Solving the second order differential equation and applying the average potential difference between the two electrodes as the boundary condition results in the potential profiles shown in Figs. 3 and 7. The relative energy difference of the valence electrons creates a potential drop between two electrode halves within the metal slab.

An applied potential induces surface charging that polarizes the water solution adjacent to the electrode. Similar to the oxygen density profiles, the comparison of potential profiles in mCF and SPC/E water at small applied potentials show that the choice of water model does not introduce noticeable differences. Under an applied potential, the potential profile of the SPC/E water has a non-zero slope in the middle of fluid, indicating that water re-orientation near the surface and alignment in the bulk region does not create an electric field large enough to overcome the applied potential. Unlike the field-free region in the electrolyte of a zero applied potential

(a) mCF water



(b) SPC/E water

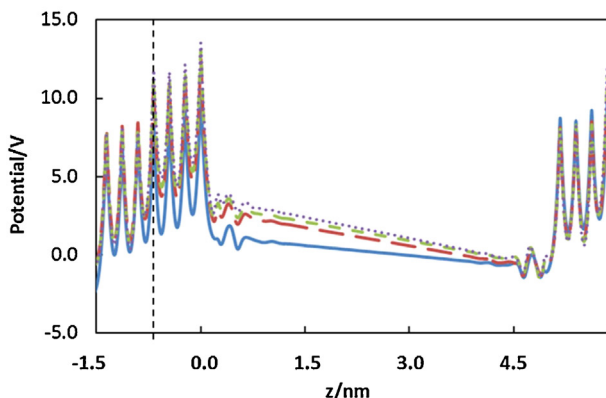


Fig. 7. The electrostatic potential profiles of (a) mCF and (b) SPC/E water models under varied applied potentials. Surface metal nuclei are located at $z=0$ (positively charged) and $z=5.2$ nm (negatively charged). The dashed lines located at $z=-0.68$ and the right border located at $z=5.88$ nm enclose a unit cell. The solid (blue) (0 V), long dashed (red) (1.25 V), short dashed (green) (1.875 V), and dotted (purple) lines (2.5 V) represent the electrostatic potential across the simulation cell at various applied potentials.

simulation or a salt solution simulation, the potential profile in the middle of the electrolyte has a slope when a potential difference is applied. Although we used a 3D-Ewald sum in the simulation, there are no spurious interactions between the electrolyte and its periodic images because the instantaneous valence charge redistribution reflects an infinite dielectric constant for the metal region, effectively screening these electrolyte-electrolyte dipole interactions. Although a sloped potential in the electrolyte region occurs for both mCF and SPC/E water, the order parameter only decays to zero for the mCF water model. This is likely due to excess hydroxyl ions in the bulk region that screen the applied potential although the simulation cell is not large enough to contain the entire diffuse layer. The effectiveness of screening at a solution/solid interface depends on the concentration of ion species, dipole-field interactions (positively charged surface), and increased number of surface water molecules (negatively charged electrode).

Dissociated water and water molecule reorientation induce surface charging and alter the capacitance of the interface. Because we do not have a constant potential bulk region, calculation of the half-cell potential drop to obtain differential capacitance is not feasible. Instead, we calculate the integral capacitance of the full cell by considering the two sides of the electrodes as a parallel plate capacitor. The calculated capacitance Cap can be used to estimate the dielectric constant ϵ , similar to experimental measurements

Table 2

Comparison of calculated capacitance (Cap) in $\mu\text{F cm}^{-2}$ and dielectric constants for water between Pt(1 1 1) electrodes.

ϵ (bulk) ^a	SPC/E			mCF water		
	Cap	ϵ^b	$\epsilon_{ }^c$	Cap	ϵ^b	$\epsilon_{ }^c$
0.00	–	–	70	–	–	51
1.25	11.84	69	67	11.69	69	51
1.87	9.29	54	62	11.47	64	–
2.50	8.75	51	54	11.14	62	–

^a ϵ (bulk) is calculated using $\epsilon = 1 + (1/(6k_BTV_{cell}\epsilon_0)) (M(t) - M(0))^2$, where M is the total dipole moment of the simulation cell, V_{cell} is the volume of simulation cell, and k_B and ϵ_0 are Boltzmann constant and vacuum permittivity [67]. The calculated ϵ for original CF water is 69.

^b ϵ is calculated using Eq. (9).

^c $\epsilon_{||}$ is calculated using Eq. (12).

where two parallel plates are filled with a dielectric medium. The dielectric constant is determined from

$$C = \frac{Q}{\Delta V} = \frac{\epsilon \epsilon_0 A}{d} \quad (9)$$

where Q denotes the surface charge on one electrode and A and d are the cross-sectional area and distance between two electrodes of the simulation cell. The calculated capacitances and dielectric constants are given in Table 2. To quantitatively compare the applied potential value with experiment is not straightforward, because the experimental measurement of potential is with respect to a standard electrode and the description of electron density of a metal electrode and water–metal interaction are approximate. The double layer capacitance from experimental measurements of a platinum electrode in 1 M potassium halide solution remains constant at $\sim 20 \mu\text{F cm}^{-2}$ before a steep rise to $\sim 40 \mu\text{F cm}^{-2}$ due to halide ion discharge at 0.4 V with respect to a standard hydrogen electrode [66]. The constant capacitance region in experiments is interpreted as a solvent capacitance. We can estimate a full cell solvent capacitance of 10 F cm^{-2} by assuming two experimental half-cell capacitors are connected in series. Our results are therefore in reasonable agreement with experiments.

The dielectric response of water molecules to the applied potential agrees with bulk water properties (see Table 1). The dielectric constant reduces with increased applied potential, consistent with a saturation effect observed in theoretical studies [4,6]. Larger dielectric constants (capacitance) for mCF than SPC/E water are observed at high-voltages because the accumulation of ion species near the charged surface induces more surface charge than pure water simulations using non-dissociative SPC/E water, although the effect is not as strong as ion specific adsorption.

The mCF water model allows water dissociation and thus provides a more realistic electrochemical interface. Hydronium and hydroxyl ions only slightly perturb the interfacial water structure, but cause substantial difference in electrostatic potential profiles compared to SPC/E water simulations. The presence of water ions also complicates the dielectric properties, for which a dynamic point of view must be considered. To further extend our analysis, we consider water dynamics between Pt electrodes.

3.4. Translational dynamics

The dynamics of water near a charged surface distinctly differ from bulk water. Strong water–platinum interactions slow water motion [1,2,68], whereas the influence of applied potential is less apparent. A simple measure of the translational mobility of interfacial water is given by the mean-square displacements (MSDs). Because of the anisotropic effect of surface confinement and applied potential, we calculate MSDs parallel and perpendicular

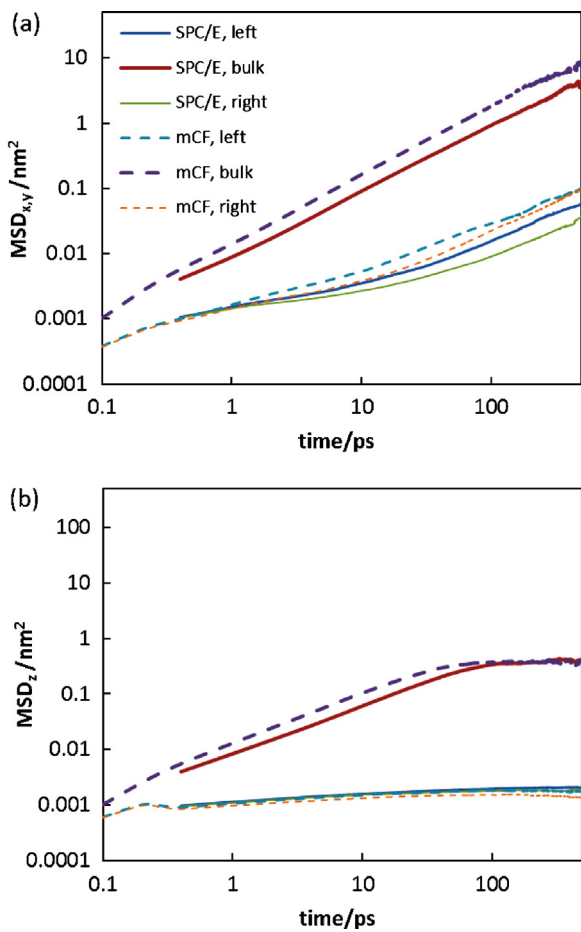


Fig. 8. Oxygen-atom MSDs of bulk and surface water layers in the direction (a) parallel and (b) normal to the surface in the absence of applied potential. The solid lines represent results from SPC/E and dashed lines represent results from mCF water simulations within bulk (thick lines), left electrode (medium lines), and right electrode (thin lines) regions. In (a), the results are the average of MSD_x and MSD_y .

to the surface. Oxygen atoms are defined as interfacial if they are in the surface region ($z=0$ – 0.4 nm for positively charged surfaces and $z=4.8$ – 5.1 nm for negatively charged surfaces) at the initial time and remain there for the entire observation time. We use a similar definition for bulk water ($z=1.5$ – 3.5 nm).

In Fig. 8 we illustrate region-dependent dynamics with the O-atom MSDs of SPC/E and mCF water as a function of box position in the absence of an applied potential. There is no significant difference in translational motion between mCF and SPC/E water. Water molecules at the surface layer are far less mobile than bulk water, with no substantial diffusion in any direction. Surface water does not become diffusive, and thus a meaningful diffusion coefficient cannot be obtained, but we provide qualitative discussions here. Water molecules are more mobile in the direction parallel (Fig. 8(a)) than normal to the surface (Fig. 8(b)), where water molecules are confined in a single water layer less than 0.4 nm in the surface normal direction. Some degree of anisotropy remains in the bulk water region.

In agreement with prior studies [2,68], applied potentials only slightly affect translational mobility of surface water (Fig. 9). The impact of applied potentials on translational dynamics is consistent with the potential-dependent interfacial structure. The in-plane mobility is dictated by the competition between surface charging and variation in the average water density of the surface layer. As shown in Fig. 9(a), the mobility of surface oxygen in the in-plane direction decreases with potential on the positively

charged surface, where the electrostatic interaction is attractive. Opposite behavior is observed on the negatively charged surface (Fig. 9(c)); oxygen mobility in the in-plane direction increases with increased potential when the surface-oxygen interaction is repulsive. Applied potential affects motion of mCF water in the surface normal direction more significantly than SPC/E water. The non-monotonic behavior of both models at the negatively charged electrode (Fig. 9(c)) results from formation of a highly dense surface water layer. In the surface normal direction (Fig. 9(b) and (d)), water mobility is dictated by the width of the first oxygen density peak; broader peaks result in larger mobility. This results in opposite behavior at the two electrodes. Surface water structure, which is altered by the applied electrode potential, plays an important role in surface water translational dynamics.

3.5. Molecular and collective orientational dynamics

Applied potential significantly influences orientation of the water dipole moment, and thus we expect a large effect on both molecular and collective water dipole dynamics. The rotational dynamics of individual water molecules are connected to hydrogen bond dynamics [69] because the rotational correlation function decays to zero only if its hydrogen bonded network is not correlated to its original state. Collective rotational-motion influences the solution dielectric properties that depend on the motion of the total dipole in the system. Similar to translational dynamics, surface confinement and layered water structure also lead to anisotropic rotational motions [1,68].

The rotational dynamics of water are investigated by computing the molecular dipole moment autocorrelation functions (ACFs, $C_\mu(t)$)

$$C_\mu(t) = \left\langle \frac{1}{N} \sum_{i=1}^N \mu_i(t) \mu_i(0) \right\rangle \quad (10)$$

where N denotes the number of water molecules, $\mu_i(t)$ is the water molecular dipole at time t , and $\langle \rangle$ signifies a time average. We calculate the ACFs of the water dipole vector parallel ($C_{\mu,xy}(t)$) and perpendicular ($C_{\mu,z}(t)$) to the surface. Water dipole reorientation is complicated by the movement of molecules between layers, which occurs on a similar time scale to water dipole relaxation. We thus do not divide the box into individual water layers to examine the impact of applied potentials on water dipole relaxation. The mCF water dipole relaxation requires the same definition of intact water molecules used in the order parameter calculation. Also, if an oxygen atom is participating in a reaction and does not meet the requirements for water (cutoff distance and HOH angle), its dipole dynamics are not counted in subsequent time steps.

As with translational mobility, the electrode surface slows the orientational dynamics of water. Fig. 10(a) and (b) shows the molecular dipole ACF as a function of applied potential and water model. The in-plane relaxation of SPC/E water (right panel in Fig. 10(a)) involves two distinct relaxations. The first occurs faster than 10 ps, and the second is much slower, with time scales \sim 1 ns. About 80% of water undergoes the fast process, with relaxation time similar to bulk water. This percentage roughly reflects the ratio of bulk free water to confined surface water. The contribution from bulk water dynamics (fast relaxation) is not affected by the applied potential, but the time associated with the slow fraction is longer under applied potentials of 1.25 and 2.5 V. The non-monotonic trend is consistent with the in-plane MSD at the negatively charged surface. As with translation, rotational dynamics of surface water in the z -direction results from a competition between surface charge and interfacial water density. The right panel in Fig. 10(b) shows that z -direction rotational dynamics are connected to applied potential,

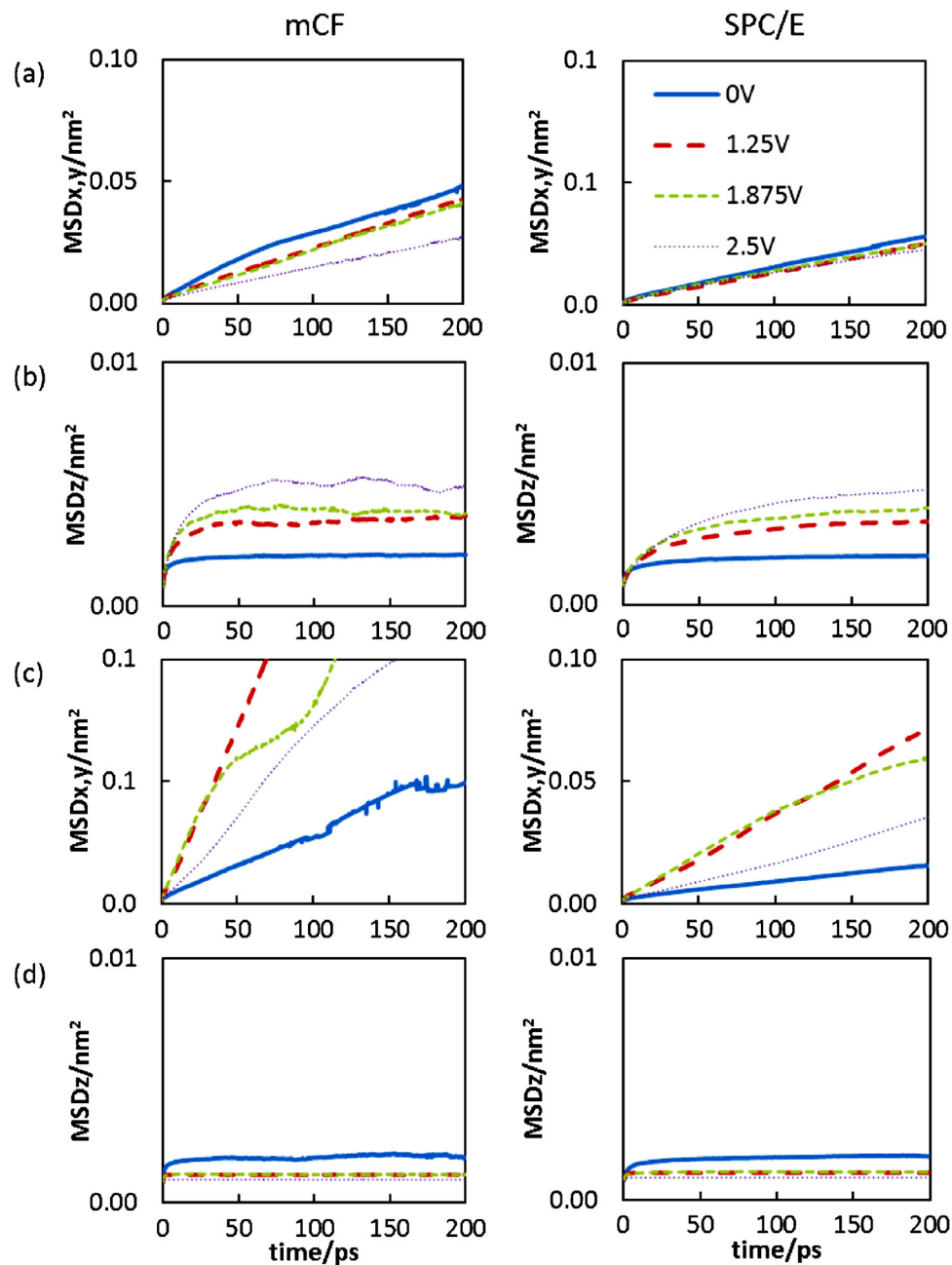


Fig. 9. Mean square displacements of oxygen atoms within surface layers in the direction (a) parallel and (b) normal to the positively charged surface, and (c) parallel and (d) normal to the negatively charged surface. The left and right panels are results from mCF and SPC/E water, respectively. The solid (blue) (0 V), long dashed (red) (1.25 V), short dashed (green) (1.875 V), and dotted (purple) (2.5 V) lines represent the MSDs at various applied potentials. In (a) and (c), the results are the average of MSD_x and MSD_y .

which limits the degree of dipole moment reorientation. The values where $C_z(t)$ levels off reflect the constraint from the applied potential. The associated relaxation times are shorter in $C_{\mu,z}(t)$.

Dissociative water complicates analysis of water dipole relaxation. The average lifetime of mCF water molecules is shorter than the time required for compete reorientation of the water dipole, meaning that a water molecule losses its identity before it completely reorients. Although we can only determine dipole relaxation within a water lifetime (several hundred picoseconds), the important trends of rotational dynamics are clear, as shown in the left panels in Fig. 10(a) for $C_{\mu,xy}(t)$ and (b) for $C_{\mu,z}(t)$. Similar to SPC/E water simulations, rotational relaxation is anisotropic with the fraction of fast mCF water similar to the relaxation of bulk mCF water. The order parameter calculations in Section 3.2 show no specific ordering in the bulk layer of mCF water under applied

potentials, but μ_z cannot reorient entirely. This result might be attributed to the surface water. The presence of ions and water flexibility enhance surface water ordering and further affect rotational dynamics. The effect is amplified with increased applied potentials.

Single molecule rotational dynamics in non-dissociative (SPC/E) and dissociative (mCF) water experience different perturbations from the electrode surface and applied potentials. The common results are similar to those reported in literature [70–72] where surface confinement slows down single water dipole relaxation in the in-plane direction and out-of-plane dipole reorientation is restricted by applied potentials. Water in an ionic environment (mCF water) does not undergo slow water dipole relaxation due to the flexible and dissociative features that give water more degrees of freedom to relax, although the drag from ions does reduce water mobility.

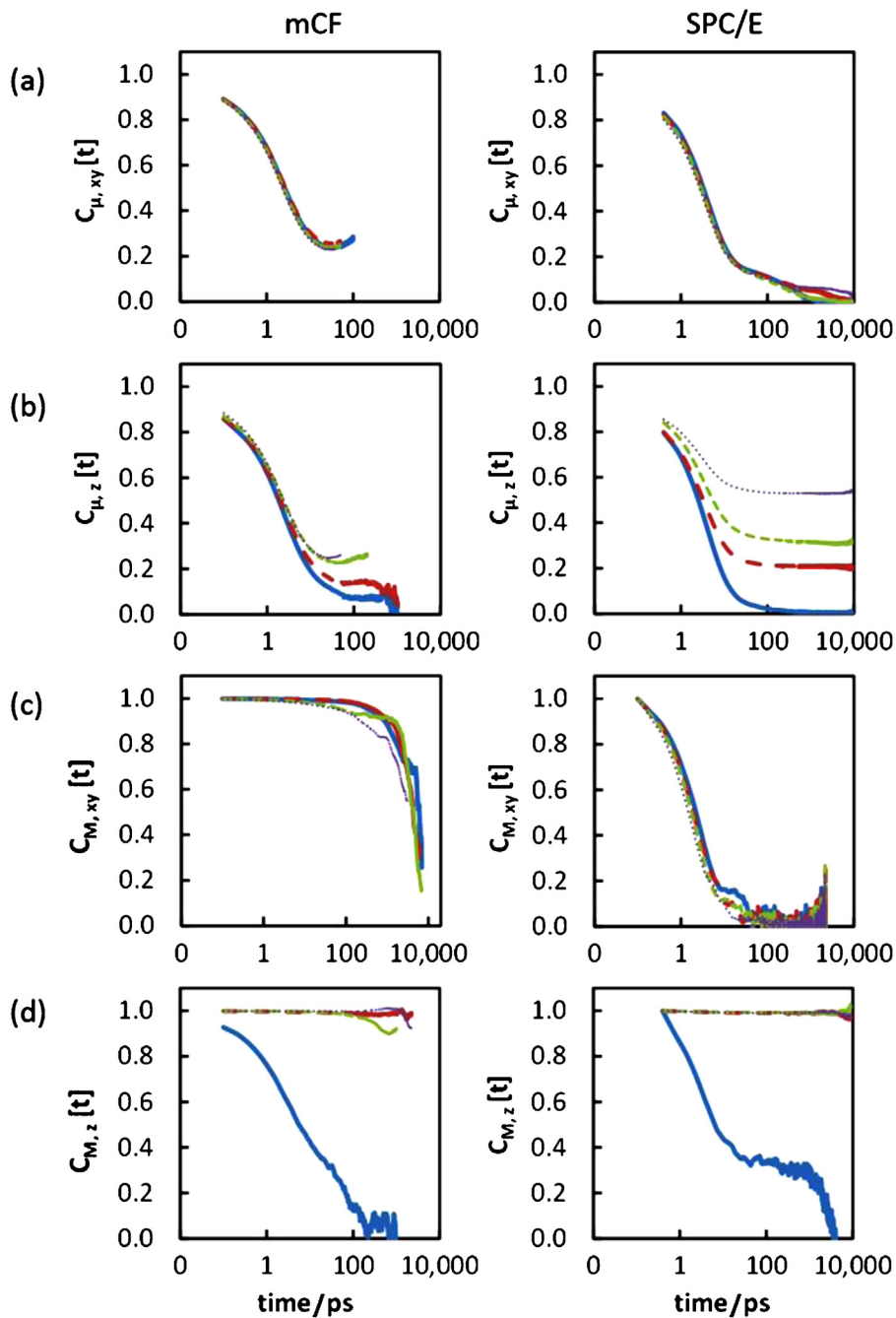


Fig. 10. Single water (a and b) and collective (c and d) dipole moment autocorrelation functions at varied applied potentials. The left panels show results from the mCF water model and right panels show results from the SPC/E water model. (a) and (c) represent results parallel to the surface direction. (b) and (d) represent results in the surface normal direction. The solid (blue) (0 V), long dashed (red) (1.25 V), short dashed (green) (1.875 V), and dotted (purple) (2.5 V) lines represent the autocorrelation functions at various applied potentials. The ACF in (a) and (b) are terminated when the time is longer than the mCF water lifetime.

The collective dipole response differs from the molecular dipole response because the collective motions are highly cooperative and involve both ions and water [76]. The total dipole ACFs, $C_M(t)$, are calculated using

$$C_M(t) = \frac{1}{N} \langle M(t)M(0) \rangle \quad (11)$$

where $M(t)$ is the total dipole moment in xy-plane or z components. The time associated with this ACF is closely related to the frequency-dependent dielectric response [73]. The right panels of Fig. 10(c) and (d) present the in-plane and out-of-plane ACFs for the SPC/E model. Parallel to the surface, $C_{M,xy}(t)$ decays to

zero, whereas the perpendicular to the surface, $C_{M,z}(t)$, is strongly suppressed under an applied potential. The long-life tail in the molecular dipole relaxation due to surface water is no longer present, leaving the overall relaxation time approximately 10 ps. This is consistent with the reported Debye relaxation time of bulk SPC/E water [67]. As expected, the relaxation time of the collective dipole is longer than the fast relaxation time associated with molecular dipole reorientation because collective dynamics is strongly coupled to the motion of neighboring water molecules [74]. The disappearance of the long-life tail seems rather counterintuitive, given that the collective motion requires longer length scale motion than single water molecule reorientation. As most of the surface

water molecules are parallel to the surface, their individual dipole moment might be arranged in a specific way that minimizes the total dipole parallel to the surface. Therefore, instead of slowing down the dipole relaxation, surface water has nearly no influence on the total dipole relaxation. However, the surface canceling effect is not valid in the surface normal direction because the applied potential aligns water in the direction against the electrical potential.

For mCF water, hydronium and hydroxyl ions accumulate at opposite sides of the electrodes, leading to out-of-plane ACFs that do not decay at all during the simulations, as seen in the left panel of Fig. 10(d). The relaxation time of the in-plane dipole (Fig. 10(c)) is approximately 10 ns under an applied potential, much slower than for SPC/E water. These differences provide measure of the in-plane dielectric properties of aqueous solution between Pt electrodes. The collective dipole moment relaxation of dissociative water (mCF) is 1000 times longer than non-dissociative water (SPC/E) both in solution and between Pt electrodes, as compared in the left and right panels in Fig. 10(c). The difference in time scale for total dipole relaxation results from different contributions to the total dipole moment. For SPC/E water, the dominant contribution is the molecular dipole, whereas for mCF water, it is water ion arrangement. The bulk static dielectric constant of mCF water also differs from SPC/E and original CF water (see Table 2). At the interface, the charged electrode, which immobilizes charged species, augments the impact of water ions on total dipole relaxation. Because only $C_{M,xy}(t)$ decays to zero, we can only determine a static dielectric constant (ϵ_{xy}) in the in-plane direction. We use [73,75]

$$\epsilon_{xy} = 1 + \frac{1}{4k_B T V_{cell} \epsilon_0} (M_{xy}(t) - M_{xy}(0))^2 \quad (12)$$

where V_{cell} is the volume of the simulation cell, and k_B and ϵ_0 are Boltzmann constant and vacuum permittivity. Results for static dielectric constants are given in Table 2, together with the corresponding bulk results. The static dielectric constant is a measurement of the total dipole moment. Although the potential is applied in the surface normal direction, the in plane dielectric constant still decreases with applied potential in SPC/E water. The microscopic origin of this phenomenon is that when water molecules align in the surface normal direction, the contribution of each individual water molecule to the in-plane direction decreases [73,76]. Although mCF water does not have permanent molecular dipoles, the attraction for ionic species toward the charged surface in the surface normal direction further suppresses the in-plane dielectric constant. We were not able to perform ϵ_{xy} calculations for applied potentials of 1.875 and 2.5 V, because the strong ion effect leads to a very slow decay of $C_{M,xy}$. As shown in Table 2, the dielectric constants calculated from capacitance and from total dipole moment differ, as expected. The former is mainly determined by the ion-electrode interaction within the interfacial region, where more electrons are induced to the surface to respond to water ions. The latter involves ion/water arrangement and diffusion, which is also perturbed by the charged electrode.

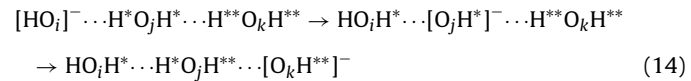
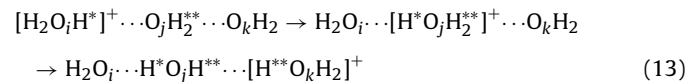
The dissociative water model not only captures water dissociation and the influence of water ions on interfacial water properties, but also enables the modeling of proton transfer near this interface, which is also crucial in fuel cell research. In the next section, we discuss the capability of our model to capture proton transfer near the electrode.

3.6. Proton transfer near the platinum electrode

Proton transfer to and from a metal electrode is a fundamental process in electrochemistry. Protons transfer through the Grotthuss hopping mechanism, which involves breaking and forming of covalent and hydrogen bonds [27]. This structural diffusion is

responsible for the high mobility of protons in aqueous solution. Compared to extensive investigations from experiments [77,78] and simulations [21,22,24,26] on H_3O transfer, OH transfer receives less attention, and the detailed structure of the solvation shell in water has not yet been fully resolved [28,79]. As mentioned in Section 1, molecular modeling of proton transfer motivates the development of reactive water models [21,22,24,26,34]. One big advantage of the mCF water model is that no additional force field parameterization is needed to describe both hydronium and hydroxyl transfer process, and it also allow us to investigate the transfer reactions on long time scales. In this section, we sketch briefly the ability of the mCF force field to allow the proton and hydroxyl transfer in bulk solution and between Pt electrodes. The impact of applied potential on charge transfer is also examined.

The charge transfer of H_3O^+ and OH^- species are described as the following reactions:



In both cases, charges are transferred from O_i to O_k via O_j . The hydrogen bonds within the transfer network are indicated by dotted lines, and H, H^* , and H^{**} denote H initially coordinated to different oxygen atoms. A H atom can shuttle between two water molecules (oxygen atoms i and j) for a period of time before a H is transferred to another oxygen atom. Events associated with H oscillation occur with a relatively short time interval. An “effective” positive charge transfer occurs only if an excess H is transferred from O_i to O_k , i.e. a new H_3O is formed, while hydroxyl ions move in the opposite sense. With H oscillation and effective charge transfer distinguished, we calculate species lifetimes. The first lifetime of hydronium and hydroxyl species is simply based on H oscillation. The time required for an effective charge transfer is a second property. For hydronium, effective charge transfer is counted by first observing O_j accepting H^* from O_i and then observing O_j giving up one of its original hydrogen (H^{**}); for hydroxyl, we first observe O_j losing one H^* and then O_j receiving one H^{**} from a different O_k .

The counts of reaction events per time indicate the reaction rate for proton transfer reaction in solution. Because the numbers of the two transfer events vary with the number of ion species, it is difficult to directly compare systems with varying ion concentrations. Hence, the effectiveness of $\text{H}_3\text{O}/\text{OH}$ transfer is defined as the ratio of the number of effective transfers (event two) to the total number of oscillation events (event one). This provides information as to how water ion distributions and interfacial water structures alter the effectiveness of charge transfer as a function of applied potential. This comparison is particularly important when hydronium/hydroxyl is transferred to a charged electrode surface because the rate-limiting step for proton transfer is the rearrangement of hydrogen bonds in the solvation shell [21], which is altered by the charged electrodes. Our definition of charge transfer effectiveness is similar to that used in ab initio MD studies of proton transfer in aqueous sulfuric acid solutions and polymer electrolyte membranes where nonconstructive and constructive proton transfer are described [80,81].

Before we discuss proton transfer near the electrode surface, we first examine proton transfer (event one) and charge transfer (event two) in the bulk solution simulation. The first event represents the lifetime of H_3O and OH , which is estimated as the time period for which an oxygen atom retains its coordination number (CN). Only oxygen that is coordinated by three hydrogen atoms ($\text{CN} = 3$)

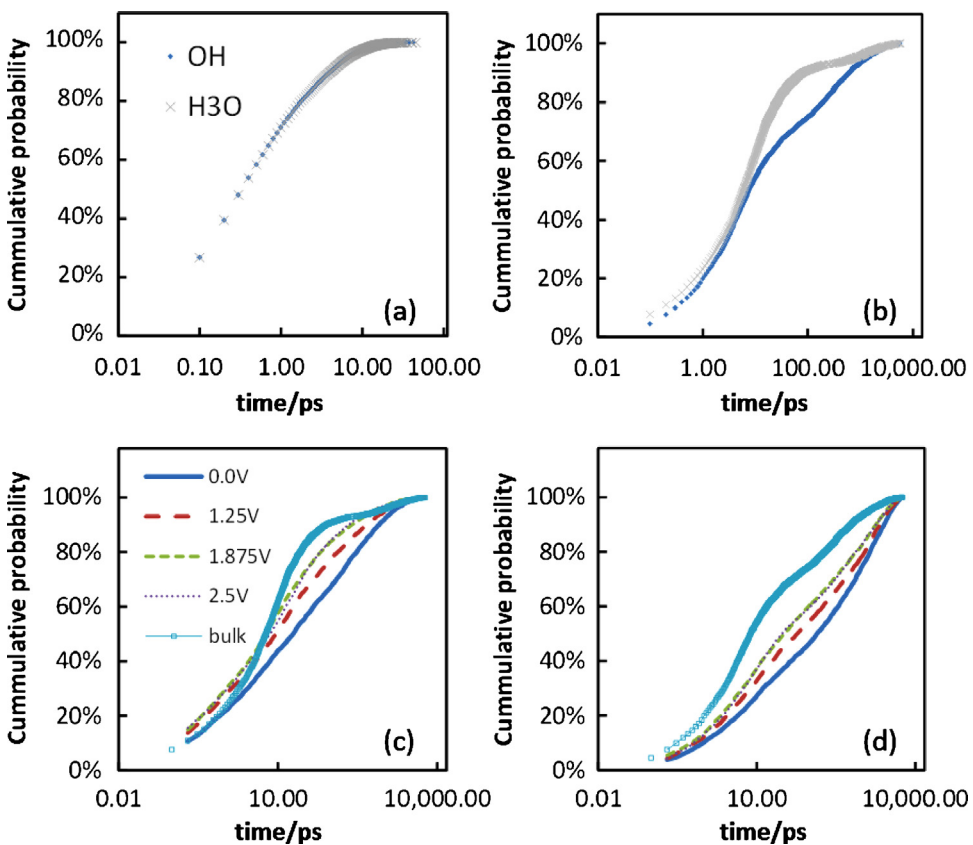


Fig. 11. The cumulative probability of (a) lifetimes and (b) effective charge transfer times for hydroxyl (light) and hydronium (dark) ions in bulk solution. The cumulative probability of the effective charge transfer times for (c) hydronium near negatively charged surfaces, and (d) hydroxyl near positively charged surfaces. Results at various applied potentials are represented in solid (blue) (0 V), long dashed (red) (1.25 V), short dashed (green) (1.875 V), and dotted (purple) (2.5 V) lines. Bulk results (thick – dark lines) from (b) are shown for comparison.

is considered as a H₃O species. OH species are defined in the same manner with CN = 1. Fig. 11(a) shows the cumulative lifetime distributions of H₃O and OH ions in bulk solution, suggesting the number (percentage) of the events that have occurred within the specified time. For example, more than 50% of H₃O or OH have lifetimes less than 0.5 ps, in agreement with vibrational spectra that indicate the time associated with proton vibration between water molecules is on the order of 100 fs [78]. As expected, the time needed for an effective charge transfer to occur is longer than H oscillation, indicating that each H that leaves/attaches does not trigger another H transfer to process a successful charge transfer. Successful transfer often requires rearrangement of the local hydrogen bonding network around a recipient oxygen atom [80]. The effectiveness for charge transfer is ~20% for both ion species in mCF water simulations, slightly lower than 31% from ab initio MD studies of sulfuric acid solution [80].

As shown in Fig. 11(b), different features are seen for the hydronium and hydroxyl's effective charge transfer although the lifetimes for both species are nearly the same. The origin of the relatively slow OH mobility is speculated to be due to the formation of a stable hydrated OH complex where oxygen prefers to form four hydrogen bonds [79]. For both ions, more than 50% of charge transfer occurs within 10 ps, but several processes take extraordinarily long time (on the order of ns). Ignoring the transfer trajectories longer than 1 ns, the average charge transfer times are 30.9 and 82.7 ps for H₃O and OH. The difference in dynamics between H₃O and OH transfer is qualitatively consistent with the fact that H₃O has faster mobility than OH in bulk solution [79]. The times associated with H oscillation (1 ps) and charge transfer (30 ps) are longer than previous ab initio studies that found 100 fs for event one and

2 ps for event two [78,80]. The one order of magnitude slower proton transfer in our simulation compared to experiments might be attributed to the use of effective partial charges with pair additive potentials and the reduced water dipole. The occurrence of hydronium and hydroxyl recombination to water might also slow down the effective charge transfer.

To investigate the influence of applied potential on charge transfer near the electrode surface, we first compare the effective charge transfer times, shown in Fig. 11(c) and (d). Here, we consider transfer events within the entire interfacial region ($Z=0.0\text{--}1.0\text{ nm}$ for positively and $4.2\text{--}5.2\text{ nm}$ for negatively charged electrodes). The electrode surface slows charge transfer due to the slow water mobility near the surface. Our model is not able to capture electron exchange between Pt and O/H atoms, and the results shown here only represent the influence of applied potentials on hydronium and hydroxyl transfer in solution. Increasing applied potential accelerates hydronium (hydroxyl) transfer on the negatively (positively) charged surfaces. Results from $\Delta V=1.875$ and 2.5 V are not discernible. When surfaces and ions carry the same type of charge, the amount of surface charge has almost no influence on the transfer times (not shown here).

The transfer effectiveness is determined by ion species lifetimes (event one) and charge transfer times (event 2). In Fig. 12, we report the effectiveness of charge transfer within the interfacial region. The effectiveness of both species under zero applied potential is greater than in bulk solution simulation (20% for both ions), which indicates that just the presence of the Pt surface improves charge transfer. The dense interfacial layers of ions and water enhance the interaction between proton-receiving and donating species, although the effective charge transfer takes longer to

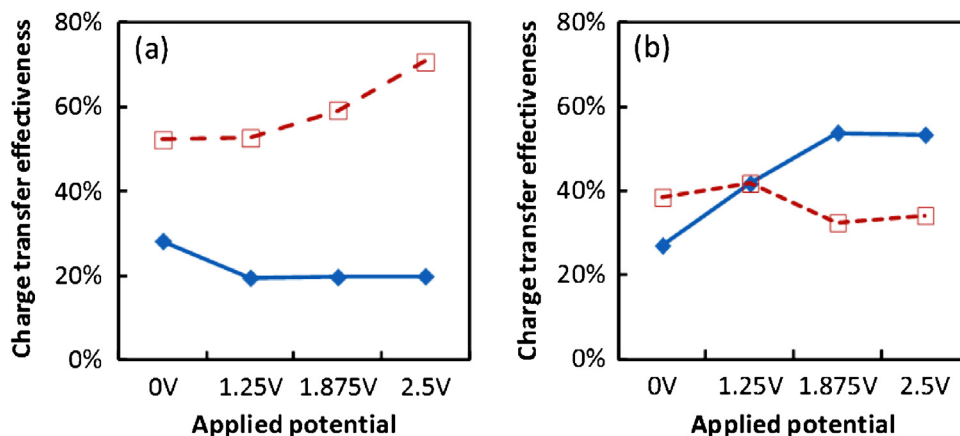


Fig. 12. The effectiveness of hydroxyl (◆ with solid line) and hydronium (□ with dashed line) transfer at (a) positively charged interfaces, and (b) negatively charged interfaces as a function of applied potential.

occur because of the slow dynamics of water arrangement. Applied potentials alter the interfacial structure and further affect charge transfer effectiveness. Positively charged surfaces provide an OH-rich interface, where OH and H₂O can interact so frequently that the number of both events increases. The hydroxyl ion lifetime increases by 40% when the potential is altered from zero to 2.5 V; however, charge transfer for hydroxyl ions only increases by 20%. Collectively, positive surface charges hinder the effectiveness of hydroxyl transfer. On the contrary, H₃O is very stable on this OH-rich interface (positively charged), and the strong H₃O-OH ionic interaction inhibits interactions between H₃O and water molecules. Although hydronium charge transfer remains constant, its lifetime decreases by 20% when a potential of 2.5 V is applied, resulting in an increased effectiveness of hydronium transfer near a positively charged surface. The same trends are observed for negatively charged electrodes, where hydroxyl transfer becomes more effective and hydronium transfer becomes less effective, as shown in Fig. 12(b). The results suggest that the presence of OH increases the frequency of H oscillation and OH charge transfer and the presence of H₃O improves H oscillation and H₃O charge transfer frequency. However, the overall effectiveness is reduced because the influence of surface charge on the denominator (H oscillation) is larger than the numerator (charge transfer).

4. Conclusions

Our study is the first molecular dynamics simulation that combines dissociative water with a potential controlled Pt(111) electrode. The use of the modified central force (mCF) water model allows for bond formation and breaking, and the electrode charge dynamics model describes electrodes with direct variation of applied potential. This allowed us to investigate the influence of hydroxyl and hydronium ions on interfacial structure and dynamics, which is important for fuel-cell-relevant electrochemistry. Water structure, dynamics, and hydronium and hydroxyl ion transfer dynamics were considered. As a comparison, the rigid SPC/E model illustrates the applied potential at which the influence of water ions on interfacial water structure and dynamics and electrochemical properties can no longer be neglected. The importance of potential-induced water dissociation is illustrated by comparing simulations between SPC/E and mCF water models. Similar structure and dynamics in SPC/E and mCF water under potentials of 0 and 1.25 V suggests that a non-dissociative water model yields reasonable interfacial properties as long as the applied potential remains low. The discrepancy in dipole moment autocorrelation, even for low applied potentials, demonstrates the need to allow

for dissociation when investigating interfacial water dynamics. The influence of hydronium and hydroxyl ions from water dissociation becomes more substantial when interfacial water molecules reach their reorientation limit. Because water ions are able to effectively screen the applied potential, interfacial properties are very sensitive to the interaction between charged surfaces and water ions. The formation of a counterion-electrode double layer results in different capacitance and dielectric properties between dissociative and non-dissociative water models at potentials of 1.875 and 2.50 V.

In mCF water, ions do not significantly influence the interfacial structure. Oxygen density distributions show that water molecules arrange in two layers adjacent to the metal surface. Hydronium and hydroxyl ion solvation influences the water layer near strongly charged surfaces. Tightly hydrated ions creating a more structured interfacial water is also observed for salt solution [11]. Proton transfer reactions in mCF water shuttle oxygen atoms between ions (OH/H₃O) and water molecules, and this responds to the field more readily than the molecular dipole alignment in SPC/E water. The lack of dipole alignment results in a weaker potential dependence of the dielectric constant in mCF water compared to SPC/E water [4,6]. In these constant potential simulations, the influence of charge on overall water orientation is smaller than simulations when a constant charge electrode is used because charges within the electrode dynamically respond to the ions nearby, limiting the influence primarily to the interfacial region. At large potentials, more ions accumulate near the charged surface, which induces more surface charge than SPC/E water reorientation. The capacitance and dielectric constant of mCF water remain nearly constant, whereas variation occurs with non-dissociative water models or a constant charge electrode.

Reactive water has an important influence on water rotational dynamics that cannot be observed in a non-reactive water model. Although proton transfer is related to water rotational dynamics (hydrogen bond decay), it is difficult to unambiguously identify oxygen identity. Our results show that there is no complete water dipole relaxation, indicating that the time required for proton transfer is shorter than water dipole relaxation. The timescales associated with dipole relaxation and proton transfer are in agreement with experiments and a sophisticated MS-EVB model [83]. Our simulations provide a reliable and more realistic picture for interfacial water dynamics in the presence of hydronium or hydroxyl ions.

The mCF water model is a realistic description of proton transfer dynamics of hydronium and hydroxyl ions in terms of lifetime and the time needed for an effective charge transfer. The longer

time required for effective charge transfer of hydroxyl compared to hydronium agrees with experimental observations that hydronium transport is faster than hydroxyl transport in solution. The slow diffusion of hydroxyl ions might also contribute to the slow hydrogen oxidation/evolution in alkaline solution compared to acidic solution [82]. The success of describing H transfer (event 1) and effective charge transfer (event 2) in bulk solution enables us to investigate the impact of applied potential on water ion transfer near the electrode surface. The local H transfer, determining lifetime of hydronium and hydroxyl species, is more sensitive to the applied potentials than the effective charge transfer, resulting in a low effectiveness of charge transfer for OH near positively or H₃O near negatively charged surfaces, although both processes are accelerated in the presence of applied potentials. Qualitatively, proton transfer and charge transfer are well represented in the mCF water model. The model can be further extended to incorporate salts or acids for a more representative electrochemical system.

Acknowledgements

The authors gratefully acknowledge the financial support from the National Science Foundation, Grant # CBET-0730502. The authors would also like to thank Dr. Lukas Vlcek for providing a modified version of the LAMMPS code and his help for the implementation of our water model into the code.

References

- [1] G. Nagy, K. Heinzinger, E. Spohr, Modelling water at platinum surfaces, *Faraday Discussions* 94 (1992) 307.
- [2] I.C. Yeh, M.L. Berkowitz, Structure and dynamics of water at water|Pt interface as seen by molecular dynamics computer simulation, *Journal of Electroanalytical Chemistry* 450 (1998) 313.
- [3] K. Raghavan, K. Foster, K. Motakabir, M. Berkowitz, The structure of water at platinum/water interfaces: molecular dynamics computer simulations, *Journal of Chemical Physics* 94 (1991) 2110.
- [4] A.P. Willard, S.K. Reed, P.A. Madden, D. Chandler, Water at an electrochemical interface – a simulation study, *Faraday Discussions* 141 (2009) 423.
- [5] C.G. Guymon, R.L. Rowley, J.N. Harb, D.R. Wheeler, Simulating an electrochemical interface using charge dynamics, *Condensed Matter Physics* 8 (2005) 335; C.G. Guymon, J.N. Harb, R.L. Rowley, D.R. Wheeler, MPSA effects on copper electrodeposition investigated by molecular dynamics simulations, *Journal of Chemical Physics* 128 (2008) 044717.
- [6] I.C. Yeh, M.L. Berkowitz, Dielectric constant of water at high electric fields: molecular dynamics study, *Journal of Chemical Physics* 110 (1999) 7935.
- [7] S. Schnur, A. Groß, Properties of metal–water interfaces studied from first principles, *New Journal of Physics* 11 (2009) 125003.
- [8] M. Otani, I. Hamada, O. Sugino, Y. Morikawa, Y. Okamoto, T. Ikeshoji, Structure of the water/platinum interface – a first principles simulation under bias potential, *Physical Chemistry Chemical Physics* 10 (2008) 3609.
- [9] O. Sugino, I. Hamada, M. Otani, Y. Morikawa, T. Ikeshoji, Y. Okamoto, First-principles molecular dynamics simulation of biased electrode/solution interface, *Surface Science* 601 (2007) 5237.
- [10] P.S. Crozier, R.L. Rowley, D. Henderson, Molecular dynamics calculations of the electrochemical properties of electrolyte systems between charged electrodes, *Journal of Chemical Physics* 113 (2000) 9202.
- [11] C.G. Guymon, M.L. Hunsaker, J.N. Harb, D. Henderson, R.L. Rowley, Effects of solvent model flexibility on aqueous electrolyte behavior between electrodes, *Journal of Chemical Physics* 118 (2003) 10195.
- [12] A. Calhoun, G.A. Voth, Electron transfer across the electrode/electrolyte interface: influence of redox ion mobility and counterions, *Journal of Physical Chemistry* 100 (1996) 10746.
- [13] M.R. Philpott, J.N. Glosli, Screening of charged electrodes in aqueous electrolytes, *Journal of the Electrochemical Society* 142 (1995) L25.
- [14] E. Wernersson, R. Kjellander, On the effect of image charges and ion-wall dispersion forces on electric double layer interactions, *Journal of Chemical Physics* 125 (2006) 154702.
- [15] J.I. Siepmann, M. Spruk, Influence of surface topology and electrostatic potential on water/electrode systems, *Journal of Chemical Physics* 102 (1995) 511.
- [16] M.K. Petersen, R. Kumar, H.S. White, G.A. Voth, A computationally efficient treatment of polarizable electrochemical cells held at a constant potential, *Journal of Physical Chemistry C* 116 (2012) 4903.
- [17] P.L. Geissler, C. Dellago, D. Chandler, J. Hutter, M. Parrinello, Autoionization in liquid water, *Science* 291 (2001) 2121.
- [18] C.W. David, Electric field assisted proton transfer in the water dimer, *Chemical Physics Letters* 78 (1981) 488.
- [19] S. Meng, Dynamical properties and the proton transfer mechanism in the wetting water layer on Pt(111), *Surface Science* 575 (2005) 300.
- [20] M. Tuckerman, K. Laasonen, M. Spruk, M. Parrinello, Ab initio molecular dynamics simulation of the solvation and transport of hydronium and hydroxyl ions in water, *Journal of Chemical Physics* 103 (1995) 150.
- [21] A.A. Kornyshev, A.M. Kuznetsov, E. Spohr, J. Ulstrup, Kinetics of proton transport in water, *Journal of Physical Chemistry B* 107 (2003) 3351.
- [22] F.H. Stillinger, C.W. David, Polarization model for water and its ionic dissociation products, *Journal of Chemical Physics* 69 (1978) 1473.
- [23] M.E. Selvan, D.J. Keffer, S. Cui, S.J. Paddison, Proton transport in water confined in carbon nanotubes: a reactive molecular dynamics study, *Molecular Simulation* 36 (2010) 568.
- [24] M.E. Selvan, D.J. Keffer, S.T. Cui, S.J. Paddison, A reactive molecular dynamics algorithm for proton transport in aqueous systems, *Journal of Physical Chemistry C* 114 (2010) 11965.
- [25] M.A. Lill, V. Helms, Reaction rates for proton transfer over small barriers and connection to transition state theory, *Journal of Chemical Physics* 115 (2001) 7985.
- [26] M.A. Lill, V. Helms, Molecular dynamics simulation of proton transport with quantum mechanically derived proton hopping rates (Q-HOP MD), *Journal of Chemical Physics* 115 (2001) 7993.
- [27] C.J.D. van Grotthuss, Sur la décomposition de l'eau et des corps qu'elle tient en dissolution à l'aide de l'électricité galvanique, *Annali di Chimica* 58 (1806) 54.
- [28] S.H. Lee, J.C. Rasaiah, Local dynamics and structure of the solvated hydroxide ion in water, *Molecular Simulation* 36 (2010) 69.
- [29] M.E. Selvan, D.J. Keffer, S. Cui, Reactive molecular dynamics study of proton transport in polymer electrolyte membranes, *Journal of Physical Chemistry C* 115 (2011) 18835.
- [30] M.K. Petersen, G.A. Voth, Characterization of the solvation and transport of the hydrated proton in the perfluorosulfonic acid membrane nafion, *Journal of Physical Chemistry B* 110 (2006) 18594.
- [31] F. Wilhelm, W. Schmickler, E. Spohr, Proton transfer to charged platinum electrodes. A molecular dynamics trajectory study, *Journal of Physics: Condensed Matter* 22 (2010) 175001.
- [32] H.L. Lemberg, F.H. Stillinger, Central force model for liquid water, *Journal of Chemical Physics* 62 (1975) 1677.
- [33] F.H. Stillinger, A. Rahman, Revised central force potentials for water, *Journal of Chemical Physics* 68 (1978) 666.
- [34] D.W.M. Hofmann, L. Kuleshova, B. D'Aguanno, A new reactive potential for the molecular dynamics simulation of liquid water, *Chemical Physics Letters* 448 (2007) 138.
- [35] A. Nyberg, A.D.J. Haymet, The dissociation of water. Analysis of the CF1 central force model of water, in: C.J. Cramer, D.G. Truhlar (Eds.), *Structure and Reactivity in Aqueous Solution: Characterization of Chemical and Biological Systems*, ACS Symposium Series, vol. 568, American Chemical Society, Washington, DC, 1994, p. 110.
- [36] D.M. Duh, D.N. Perera, A.D.J. Haymet, Structure and properties of the CF1 central force model of water: integral equation theory, *Journal of Chemical Physics* 102 (1995) 3736.
- [37] D.W.M. Hofmann, L. Kuleshova, B. D'Aguanno, Molecular dynamics simulation of hydrated Nafion with a reactive force field for water, *Journal of Molecular Modeling* 14 (2008) 225.
- [38] H.J.C. Berendsen, J.R. Grigera, T.P. Straatsma, The missing term in effective pair potentials, *Journal of Physical Chemistry* 91 (1987) 6269.
- [39] A.K. Soper, The radial distribution functions of water and ice from 220 to 673 K and at pressures up to 400 MPa, *Chemical Physics* 258 (2000) 121.
- [40] K. Ichikawa, Y. Kameda, T. Yamaguchi, H. Wakita, M. Misawa, Neutron-diffraction investigation of the intramolecular structure of a water molecule in the liquid phase at high temperatures, *Molecular Physics* 73 (1991) 79.
- [41] Y.S. Badyal, M.L. Saboungi, D.L. Price, S.D. Shastri, D.R. Haefner, A.K. Soper, Electron distribution in water, *Journal of Chemical Physics* 112 (2000) 9206.
- [42] W.S. Price, H. Ide, Y. Arata, Self-diffusion of supercooled water to 238 K using PGSE NMR diffusion measurements, *Journal of Physical Chemistry A* 103 (1999) 448.
- [43] C.M. Payne, X. Zhao, P.T. Cummings, Electrophoresis of ssDNA through nanoelectrode gaps from molecular dynamics: impact of gap width and chain length, *Journal of Physical Chemistry B* 112 (2008) 12851.
- [44] C.M. Payne, X. Zhao, L. Vlcek, P.T. Cummings, Molecular dynamics simulation of ss-DNA translocation between copper nanoelectrodes incorporating electrode charge dynamics, *Journal of Physical Chemistry B* 112 (2008) 1712.
- [45] S. Meng, E.G. Wang, S.W. Gao, Water adsorption on metal surfaces: a general picture from density functional theory studies, *Physical Review B* 69 (2004) 195404.
- [46] A. Michaelides, V.A. Ranea, P.L. de Andres, D.A. King, General model for water monomer adsorption on close-packed transition and noble metal surfaces, *Physical Review Letters* 90 (2003) 216102.
- [47] G. Kresse, J. Furthmüller, Efficient iterative schemes for ab initio total-energy calculations using a plane wave basis set, *Physical Review B* 54 (1996) 11169.
- [48] G. Kresse, J. Furthmüller, Efficiency of ab-initio total energy calculations for metals and semiconductors using a plane-wave basis set, *Computation Materials Science* 6 (1996) 15.
- [49] G. Kresse, J. Hafner, Ab initio molecular dynamics for liquid metals, *Physical Review B* 47 (1993) 558.
- [50] P.E. Blöchl, Projector augmented-wave method, *Physical Review B* 50 (1994) 17953.

- [51] J.P. Perdew, K. Burke, M. Ernzerhof, Generalized gradient approximation made simple, *Physical Review Letters* 77 (1996) 3865.
- [52] J.P. Perdew, J.A. Chevary, S.H. Vosko, K.A. Jackson, M.R. Pederson, D.J. Singh, C. Fiolhais, Atoms, molecules, solids, and surfaces: applications of the generalized gradient approximation for exchange and correlation, *Physical Review B* 46 (1992) 6671.
- [53] S. Plimpton, Fast parallel algorithms for short-range molecular dynamics, *Journal of Computational Physics* 117 (1995) 1.
- [54] S. Plimpton, LAMMPS Molecular Dynamics Simulator Web page, 2007, <http://lammps.sandia.gov>
- [55] M.P. Allen, D.J. Tildesley, *Computer Simulation of Liquids*, Oxford University Press, New York, 1987.
- [56] S. Nose, A unified formulation of the constant temperature molecular dynamics methods, *Journal of Chemical Physics* 81 (1984) 511.
- [57] W.G. Hoover, Canonical dynamics: equilibrium phase-space distributions, *Physical Review A* 31 (1985) 1695.
- [58] P. Mark, L. Nilsson, Structure and dynamics of the TIP3P, SPC, and SPC/E water models at 298 K, *Journal of Physical Chemistry A* 105 (2001) 9954.
- [59] R.W. Hockney, J.W. Eastwood, *Computer Simulation Using Particles*, Institute of Physics, Bristol, 1998.
- [60] E. Spohr, Computer simulation of the structure of the electrochemical double layer, *Journal of Electroanalytical Chemistry* 450 (1998) 327.
- [61] S.J. Suresh, Disruption of hydrogen bond structure of water near charged electrode surfaces, *Journal of Chemical Physics* 126 (2007) 204705.
- [62] V.A. Frolov, S.H.L. Klapp, Anisotropic dynamics of dipolar liquids in narrow slit pores, *Journal of Chemical Physics* 124 (2006) 134701.
- [63] R. Guidelli, W. Schmickler, Recent developments in models for the interface between a metal and an aqueous solution, *Electrochimica Acta* 45 (2000) 2317.
- [64] M. Watanabe, A.M. Brodsky, W.P. Reinhardt, Dielectric properties and phase transitions of water between conducting plates, *Journal of Physical Chemistry* 95 (1991) 4593.
- [65] A. Kohlmeyer, W. Witschel, E. Spohr, Molecular dynamics simulations of water/metal and water/vacuum interfaces with a polarizable water model, *Chemical Physics* 213 (1996) 211.
- [66] M.A.V. Devanath, K. Ramakris, Differential capacitance of some solid metal/aqueous-electrolyte interfaces, *Electrochimica Acta* 18 (1973) 259.
- [67] P. Hochtl, S. Boresch, W. Bitomsky, O. Steinhauser, Rationalization of the dielectric properties of common three-site water models in terms of their force field parameters, *Journal of Chemical Physics* 109 (1998) 4927.
- [68] E. Spohr, Molecular dynamics simulations of water and ion dynamics in the electrochemical double layer, *Solid State Ionics* 150 (2002) 1.
- [69] D.E. Rosenfeld, C.A. Schmuttenmaer, Dynamics of the water hydrogen bond network at ionic, nonionic, and hydrophobic interfaces in nanopores and reverse micelles, *Journal of Physical Chemistry B* 115 (2011) 1021.
- [70] M.R. Harpham, B.M. Ladanyi, N.E. Levinger, The effect of the counterion on water mobility in reverse micelles studied by molecular dynamics simulations, *Journal of Physical Chemistry B* 109 (2005) 16891.
- [71] J. Faeder, M.V. Albert, B.M. Ladanyi, Molecular dynamics simulations of the interior of aqueous reverse micelles: a comparison between sodium and potassium counterions, *Langmuir* 19 (2003) 2514.
- [72] J. Faeder, B.M. Ladanyi, Molecular dynamics simulations of the interior of aqueous reverse micelles, *Journal of Physical Chemistry B* 104 (2000) 1033.
- [73] V.A. Frolov, S.H.L. Klapp, Dielectric response of polar liquids in narrow slit pores, *Journal of Chemical Physics* 126 (2007) 114703.
- [74] A.Y. Zasetsky, S.V. Petelina, A.K. Lyashchenko, A.S. Lileev, Computer simulation study of rotational diffusion in polar liquids of different types, *Journal of Chemical Physics* 133 (2010) 134502.
- [75] V. Ballenegger, J.P. Hansen, Dielectric permittivity profiles of confined polar fluids, *Journal of Chemical Physics* 122 (2005) 114711.
- [76] P.D. Duncan, P.J. Camp, Structure and dynamics in a monolayer of dipolar spheres, *Journal of Chemical Physics* 121 (2004) 11322.
- [77] K.J. Tielrooij, R.L.A. Timmer, H.J. Bakker, M. Bonn, Structure dynamics of the proton in liquid water probed with terahertz time-domain spectroscopy, *Physical Review Letters* 102 (2009) 198303.
- [78] S. Woutersen, H.J. Bakker, Ultrafast vibrational and structural dynamics of the proton in liquid water, *Physical Review Letters* 96 (2006) 138305.
- [79] D. Marx, Proton transfer 200 years after von Grotthuss: insights from ab initio simulations, *ChemPhysChem* 8 (2007) 209.
- [80] Y.-K. Choe, E. Tsuchida, T. Ikeshoji, First-principles molecular dynamics study on aqueous sulfuric acid solutions, *Journal of Chemical Physics* 126 (2007) 154510.
- [81] Y.-K. Choe, E. Tsuchida, T. Ikeshoji, S. Yamakawa, S.-A. Hyodo, Nature of proton dynamics in a polymer electrolyte membrane, nafion: a first-principles molecular dynamics study, *Physical Chemistry Chemical Physics* 11 (2009) 3892.
- [82] W.C. Sheng, H.A. Gasteiger, Y. Shao-Horn, Hydrogen oxidation and evolution reaction kinetics on platinum: acid vs alkaline electrolytes, *Journal of the Electrochemical Society* 157 (2010) B1529.
- [83] M.K. Petersen, A.J. Hatt, G.A. Voth, Orientational dynamics of water in the Nafion polymer electrolyte membrane and its relationship to proton transport, *Journal of Physical Chemistry B* 112 (2008) 7754.